

Enhancement of non-Gaussianity and nonclassicality of pair coherent states with postselected von Neumann measurement

Yi-Fang Ren^{1§}, Janarbek Yuanbek^{1§}, and Yusuf Turek^{1*}

¹*School of Physics, Liaoning University, Shenyang, Liaoning 110036, China*

(Dated: December 18, 2024)

We investigate the effects of postselected von Neumann measurements on the nonclassical properties of pair coherent states (PCS). We calculated key quantum characteristics, such as squeezing, photon statistics, and entanglement between the two PCS modes. Our results demonstrate that postselected von Neumann measurements enhance both the non-Gaussianity and nonclassicality of PCS. These findings are validated by analyzing the scaled joint Wigner function across various system parameters. The theoretical optimization scheme offers an alternative approach for improving PCS-based quantum information efficiency and facilitates practical implementations in quantum technologies.

I. INTRODUCTION

The nonclassicality of quantum states plays a crucial role in quantum computation and information processing. Recent advancements in technology allow the manipulation of photons, making continuous-variable states of bosonic modes an excellent platform for quantum information processing. Among the variety of continuous-variable states [1–3], two-mode Gaussian and non-Gaussian states such as entangled cat states [4], NOON states [5, 6], squeezed states [7, 8], and pair coherent states (PCS) [9] have irreplaceable roles in numerous applications [10–18]. In two-mode nonclassical states, enhancing nonclassicality and entanglement properties can be achieved through photon addition and subtraction operations [19–31]. However, operating with non-Gaussian states introduces additional computational complexity compared to Gaussian states. Beyond photon addition and subtraction (or their superpositions) [32], quantum catalysis provides another feasible method for enhancing the nonclassicality of quantum states [29]. Quantum catalysis enhances quantum properties without directly altering the photon count. This enhancement arises from the inherently quantum mechanical nature of the process (for further details, refer to [33], and references therein). However, quantum catalysis is not universally applicable to all states, necessitating alternative methods for optimizing nonclassical states. Specifically, exploring new state-optimization schemes is essential for improving the efficiency of multimode state-based applications—such as multimode Gaussian and non-Gaussian states—without relying on photon addition or subtraction operations.

The process of optimizing quantum states relates to the measurement problems. It requires modifying and effectively manipulating measurement procedures to enhance the properties of a given state using quantum control techniques [34]. Quantum weak measurements (WMs)

[35], a novel class of generalized measurement methods, offer feasible and effective pathways for optimizing quantum states for specific tasks. Unlike the strong measurements, WMs involve a weak coupling between the measured system and the measuring device, which prevents the destruction of the system's initial state. While a single trial of a WM does not yield precise information about the system, repeated measurements combined with post-selection allow for the statistical extraction of desired observable information. The extracted weak value is a complex quantity that can lie outside the eigenvalue spectrum of the observable [36, 37]. This phenomenon, known as weak value amplification (WVA), is useful for amplifying weak signals in quantum systems [38] (for further insights into WM theory and its applications, readers may consult the works of Nori [39] and Boyd [40]). The utility of quantum WM techniques in state preparation [41] and optimization processes has been demonstrated for various quantum states and optimization processes has been demonstrated for various quantum states [42, 43]. However, their advantages for multimode continuous-variable states of bosonic modes remain largely unexplored. For instance, while single-mode coherent states are typical semiclassical states that minimize (and equalize) the uncertainty product of two incompatible operators, PCS serve as two-mode analogs of Glauber coherent states. PCS are eigenstates of the pair-photon annihilation operator and represent a promising candidate for applying quantum WM-based state optimization methods.

In this work, we investigate how the properties of PCS change after applying the theory of postselected measurements to one mode of PCS. We calculate the squeezing, quantum statistics, and entanglement characteristics of the measurement output state. Our results show that postselected von Neumann measurements could enhance the non-Gaussianity and nonclassicality of PCS, considering large weak values of the measured system observable and appropriate coupling strength parameters between the measured system and measuring device (MD). We confirm these findings by examining the phase-space distribution of our state, characterized by the scaled joint

§ These authors contributed equally to this work.

* yusuftu1984@hotmail.com

Wigner function.

We organized the paper as follows: In Sec. II, we present our theoretical model. Section III explores the effects of postselection on the squeezing properties of PCS, including quadrature and sum squeezing. In Sec. IV, we investigate the quantum statistics of postselected PCS under von Neumann measurements, analyzing the relationship between the a -mode and b -mode using the second-order cross-correlation (SOCC) and second-order correlation functions. Section V examines entanglement through measures such as the Hillery-Zubairy (HZ) correlation and Einstein-Podolsky-Rosen (EPR) correlation. In Sec. VI, we investigate the scaled joint Wigner function of our measurement output state and take comparison with the initial PCS case. Section VII explores the fidelity of the postselected PCS under von Neumann measurements. Finally, Sects. VIII and IX present a discussion and conclusion, respectively. Throughout this paper, we take $\hbar = 1$.

II. MODEL SETUP

The coherent state is a typical semi-classical state that minimizes (and equalizes) the uncertainty product of two incompatible operators. However, the Gaussian profile characterizing the classicality of coherent states transforms into a non-Gaussian profile upon the addition of a single photon. Beyond the standard coherent state and the single-photon-added coherent state, there also exist two-mode entangled coherent states, commonly referred to as PCS [44].

Analogous to the usual coherent state, defined as $|\alpha\rangle = e^{-|\alpha|^2/2} \sum_n \alpha^n / \sqrt{n!} |n\rangle$, the PCS are a superposition of twin-Fock state bases $|n+\delta\rangle_a |n\rangle_b$ of two harmonic oscillators (a and b):

$$|\gamma, \delta\rangle = \mathcal{N}_n \sum_{n=0}^{\infty} \frac{\gamma^{n+\delta/2}}{\sqrt{n!(n+\delta)!}} |n+\delta\rangle_a |n\rangle_b. \quad (1)$$

Here, γ is a complex number representing the amplitude and phase of the state, i.e., $\gamma = re^{i\varphi}$; δ is an integer denoting the photon number difference (PND) between the two modes; and \mathcal{N}_n is a normalization coefficient defined by:

$$\mathcal{N}_n = \left(\sum_{n=0}^{\infty} \frac{|\gamma|^{2n+\delta}}{n!(n+\delta)!} \right)^{-\frac{1}{2}} = \frac{1}{\sqrt{I_\delta(2|\gamma|)}}. \quad (2)$$

Here, $I_\delta(2|\gamma|)$ denotes the modified Bessel function of the first kind, expressed as follows:

$$I_\delta(x) = \sum_{n=0}^{\infty} \frac{1}{n!(n+\delta)!} \left(\frac{x}{2}\right)^{2n+\delta}. \quad (3)$$

This state is an eigenstate of the pair-photon annihilation operator ab and the PND operator $a^\dagger a - b^\dagger b$:

$$ab|\gamma, \delta\rangle = \gamma|\gamma, \delta\rangle, \quad (4)$$

$$(a^\dagger a - b^\dagger b)|\gamma, \delta\rangle = \delta|\gamma, \delta\rangle. \quad (5)$$

Here, a (a^\dagger) and b (b^\dagger) are the annihilation (creation) operators associated with the two modes (a -mode and b -mode) of the PCS, respectively. The realization of PCS and the study of its characteristics have been achieved experimentally [45]. PCS are a type of two-mode non-Gaussian and nonclassical states [20], and their generations have been investigated both theoretically [9, 46–50] and experimentally [45, 51]. The sub-Poissonian statistics, correlations in number fluctuations, squeezing, and violations of Cauchy-Schwarz inequalities (CSI) have been studied extensively [28, 30, 44, 52, 53]. As non-Gaussian entangled states, PCS offers advantages in performing quantum tasks such as quantum communication [10, 54, 55] and quantum key distribution [12, 15].

To study the effects of postselected von Neumann measurement on the PCS, we consider the PCS as the MD (measuring device) and its polarization as the measured system. As illustrated in Fig. 1, we simplify the setup by restricting the interaction between the MD and the measured system to the a -mode. The interaction Hamiltonian H_{int} is of the von Neumann type, expressed as:

$$H_{int} = g\sigma_x \otimes P_x. \quad (6)$$

Here, g denotes the interaction strength between the MD and the measured system. The operator $\sigma_x = |D\rangle\langle D| - |A\rangle\langle A|$ represents the observable of the measured system, where $|D\rangle = \frac{1}{\sqrt{2}}(|H\rangle + |V\rangle)$, and $|A\rangle = \frac{1}{\sqrt{2}}(|H\rangle - |V\rangle)$ correspond to the diagonal and anti-diagonal polarizations of the beam, respectively. Here, $|H\rangle$ and $|V\rangle$ denote the horizontal and vertical polarizations of photons. In the interaction Hamiltonian, P_x represents the canonical momentum of the MD and can be expressed in terms of annihilation and creation operators as follows:

$$P_x = \frac{i}{2\sigma} (a^\dagger - a), \quad (7)$$

where $\sigma = \sqrt{1/2m\omega}$ represents the beamwidth. We now assume that the composite system is initially prepared in the following form:

$$|\Psi_{in}\rangle = |\psi_i\rangle \otimes |\phi\rangle, \quad (8)$$

where $|\psi_i\rangle = \cos \frac{\alpha}{2} |H\rangle + e^{i\vartheta} \sin \frac{\alpha}{2} |V\rangle$ and $|\phi\rangle = |\gamma, \delta\rangle$. As shown in Fig. 1, $|\psi_i\rangle$ and $|\phi\rangle$ represent the states of the measured system and the MD, respectively. The initial state is thus the product state between the measured system and the MD. Here, $\vartheta \in [0, 2\pi]$ and $\alpha \in [0, \pi]$. Experimentally, this type of initial state can be prepared by passing the beam through a quarter-wave and half-wave plates with appropriate optical axis angles. The

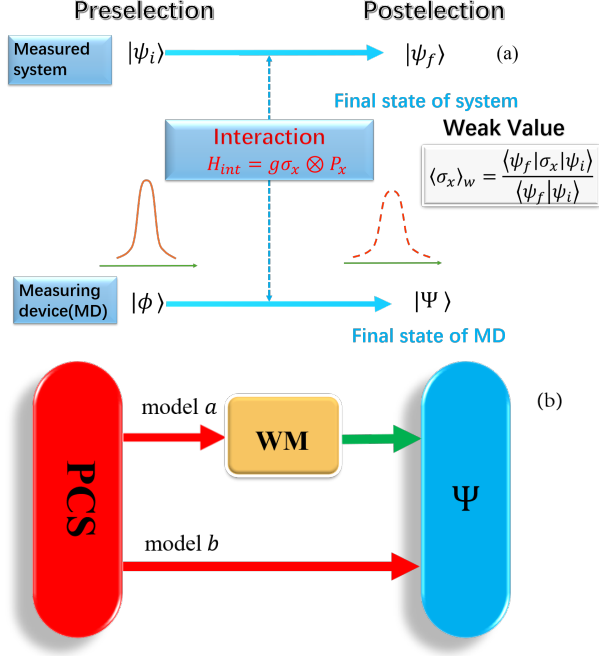


Figure 1. (a) Schematic diagram of weak measurement (WM) theory. The standard process of WM involves four steps: 1. *Preparation*: The initial state of the measured system is prepared as $|\psi_i\rangle$, while the MD is initialized in the state $|\phi\rangle$. 2. *Weak Interaction*: A weak interaction occurs between the measured system and the MD, during which the composite system evolves according to the Hamiltonian $H_{int} = g\sigma_x \otimes P_x$. Here, the coupling constant g characterizes the bilinear coupling. 3. *Postselection*: After evolution, the entire system is projected onto the postselected state $|\psi_f\rangle$. This step extracts the desired observable values of the system by selecting a specific subensemble of samples before the final measurement. 4. *Readout*: The measurement result determines the shifts in the MD. In the postselected weak measurement process, the observable value is a function of the weak value. The real (*Re*) and imaginary (*Im*) parts of the weak value are derived from the shifts in the canonical position and momentum of the MD respectively. (b) Schematic setup for preparing $|\Psi\rangle$ via postselected von Neumann measurement. Experimentally, the pointer is initially in the PCS. Using the WM strategy, where the interaction is restricted to the *a*-mode, we investigate the effects of this measurement on the properties of the PCS.

joint state, expressed in Eq. (8), evolves over time under the influence of the time evolution operator $U(t) = \exp\left(-i \int_0^t H_{int} d\tau\right)$, as follows:

$$\begin{aligned} |\Psi_{evol}\rangle &= \exp\left(-i \int_0^t H_{int} d\tau\right) |\Psi_{in}\rangle \\ &= \frac{1}{2} \left[(\mathbb{I} + \sigma_x) D\left(\frac{\Gamma}{2}\right) + (\mathbb{I} - \sigma_x) D^\dagger\left(\frac{\Gamma}{2}\right) \right] \\ &\quad \times |\psi_i\rangle \otimes |\phi\rangle. \end{aligned} \quad (9)$$

where $\Gamma = gt/\sigma$ represents the ratio between gt and σ , \mathbb{I} is the 2×2 identity matrix, and $D(\Gamma/2) = e^{\frac{\Gamma}{2}(\hat{a}^\dagger - \hat{a})}$ is

the displacement operator acting on the *a* mode of the PCS. It is important to note that the coupling strength parameter Γ characterizes the measurement strength in this study. The measurement is referred to as weak when $\Gamma \ll 1$ and strong when $\Gamma \gg 1$. For this reason, Γ can be considered the transaction parameter in our measurement model. The measurement process involves postselection. In this study, we assume the postselection of the system state to be $|\psi_f\rangle = |H\rangle$. After postselecting the system state, the final state of the MD is obtained, and its expression is given as

$$|\Psi\rangle = \frac{\lambda}{2} \left[(1 + \langle \sigma_x \rangle_w) D\left(\frac{\Gamma}{2}\right) + (1 - \langle \sigma_x \rangle_w) D^\dagger\left(\frac{\Gamma}{2}\right) \right] |\phi\rangle. \quad (10)$$

Here, λ is the normalization coefficient given by

$$\lambda = \frac{\sqrt{2}}{[1 + |\langle \sigma_x \rangle_w|^2 + (1 - |\langle \sigma_x \rangle_w|^2)P]^{\frac{1}{2}}}, \quad (11)$$

with $P = \mathcal{N}_n^2 e^{-\frac{\Gamma^2}{2}} \sum_{n=0}^{\infty} \left[\frac{|\gamma|^{2n+\delta}}{n!(n+\delta)!} L_{n+\delta}^{(0)}(\Gamma^2) \right]$, and $\langle \sigma_x \rangle_w$ is the weak value of the system observable σ_x defined as

$$\langle \sigma_x \rangle_w = \frac{\langle \psi_f | \sigma_x | \psi_i \rangle}{\langle \psi_f | \psi_i \rangle} = e^{i\vartheta} \tan \frac{\alpha}{2}. \quad (12)$$

For simplify, we assume the weak value to be a real number by setting $\vartheta = 0$. This weak value can be obtained in a measurement process with a postselection probability given by $P_s = |\langle \psi_f | \psi_i \rangle|^2 = \cos^2(\frac{\alpha}{2})$. In calculating the normalization coefficient λ , the following expressions were used

$$\langle n+d | D(\alpha) | n \rangle = \sqrt{\frac{n!}{(n+d)!}} e^{-\frac{|\alpha|^2}{2}} \alpha^d L_n^{(d)}(|\alpha|^2), \quad (13)$$

$$\langle n | D(\alpha) | n+d \rangle = \sqrt{\frac{n!}{(n+d)!}} e^{-\frac{|\alpha|^2}{2}} (-\alpha^*)^d L_n^{(d)}(|\alpha|^2), \quad (14)$$

where d is natural number, and $L_n^{(d)}(|\alpha|^2)$ represents the associated Laguerre polynomials, given by

$$L_n^{(d)}(|\alpha|^2) = \sum_{m=0}^n (-1)^m C_{n+d}^{m+d} \frac{|\alpha|^{2m}}{m!}. \quad (15)$$

Next, we examine the effects of postselected von Neumann measurement and the weak values of the measured system's observable on the inherent properties of the PCS $|\phi\rangle$.

III. THE EFFECTS ON SQUEEZING

In this section, we investigate the effects of postselected von Neumann measurement on the squeezing properties of the PCS by examining both quadrature squeezing and sum squeezing.

A. Quadrature squeezing

In continuous-variable quantum optics, quadrature squeezing is a crucial characteristic of nonclassical radiation fields, playing a vital role in the implementation of various quantum computation and communication protocols [56]. Here, we analyze how postselected von Neumann measurement influences the quadrature squeezing of the PCS.

For a single-mode radiation field, squeezing refers to the reduction of the quadrature variance below the shot noise level, i.e., $\Delta^2 X_\epsilon < \frac{1}{4}$. The quadrature operator with phase ϵ is defined as: $X_\epsilon = \frac{1}{2} (e^{-i\epsilon} a + e^{i\epsilon} a^\dagger)$, where its variance is given by: $\Delta^2 X = \langle X^2 \rangle - \langle X \rangle^2$. Similarly, for two-mode radiation fields, the quadrature operators can be defined as [57]:

$$F_1 = \frac{1}{2^{3/2}} [e^{-i\epsilon}(a+b) + e^{i\epsilon}(a^\dagger + b^\dagger)], \quad (16)$$

$$F_2 = \frac{1}{2^{3/2}i} [e^{-i\epsilon}(a+b) + e^{i\epsilon}(a^\dagger + b^\dagger)]. \quad (17)$$

They satisfy the commutation relation $[F_1, F_2] = \frac{i}{2}$, and the uncertainty relation for their fluctuations is

$$\Delta^2 F_1 \Delta^2 F_2 \geq \frac{1}{16}, \quad (18)$$

where $\Delta F_i^2 = \langle F_i^2 \rangle - \langle F_i \rangle^2$. Similar to the single-mode case, two-mode squeezing occurs when one of the variances $\Delta^2 F_i$ is below the shot noise level, i.e., $\Delta^2 F_i < 0.25$ ($i = 1, 2$). This condition can be satisfied if the two modes are uncorrelated, with one or both of F_i individually squeezed, or when nonclassical correlations, such as entanglement between the two modes, are present. We use the squeezing parameter to characterize the squeezing of the quadrature as follows:

$$Q_i = \Delta F_i^2 - \frac{1}{4}. \quad (19)$$

As we can see, the values of Q_i are bounded as $Q_i \geq -\frac{1}{4}$, and the i -th component of the quadrature operators of the PCS is said to be squeezed if $-\frac{1}{4} \leq Q_i < 0$. After some algebra, we can obtain the specific expressions for the quadrature squeezing parameter Q_i of the final state $|\Psi\rangle$, expressed as:

$$\begin{aligned} Q_{1,\Psi} &= \frac{1}{4} [\langle a^\dagger a \rangle + \langle b^\dagger b \rangle + Re[\langle a^2 \rangle] + Re[\langle b^2 \rangle]] \\ &\quad + \frac{1}{2} [Re[\langle ab \rangle] + Re[\langle a^\dagger b \rangle]] \\ &\quad - \frac{1}{2} [Re[\langle a \rangle] + Re[\langle b \rangle]]^2, \end{aligned} \quad (20)$$

and

$$\begin{aligned} Q_{2,\Psi} &= \frac{1}{4} [\langle a^\dagger a \rangle + \langle b^\dagger b \rangle + Re[\langle a^2 \rangle] + Re[\langle b^2 \rangle]] \\ &\quad - \frac{1}{2} [Re[\langle ab \rangle] - Re[\langle a^\dagger b \rangle]] \\ &\quad - \frac{1}{2} [Im[\langle a \rangle] + Im[\langle b \rangle]]^2. \end{aligned} \quad (21)$$

Here, $\langle \dots \rangle$ represents the expectation value of the associated operators under the postselected state $|\Psi\rangle$, while Re and Im denote its real and imaginary parts. Additionally, we set $\epsilon = 0$. The Appendix A provides analytic expressions for the expectation values of the associated operators. If we set $\Gamma = 0$, the above two expressions reduce to $Q_{1,\phi}$ and $Q_{2,\phi}$, corresponding to the initial MD state $|\phi\rangle$ defined in Eq. (1), and expressed as

$$Q_{1,\phi} = \frac{1}{4} \left(\frac{|\gamma| I_{\delta-1}(2|\gamma|)}{I_\delta(2|\gamma|)} + \frac{|\gamma| I_{\delta+1}(2|\gamma|)}{I_\delta(2|\gamma|)} + 2Re[\gamma] \right), \quad (22)$$

and

$$Q_{2,\phi} = \frac{1}{4} \left(\frac{|\gamma| I_{\delta-1}(2|\gamma|)}{I_\delta(2|\gamma|)} + \frac{|\gamma| I_{\delta+1}(2|\gamma|)}{I_\delta(2|\gamma|)} - 2Re[\gamma] \right), \quad (23)$$

Here, $I_\delta(2|\gamma|)$ is the modified Bessel function defined in Eq. (3). From $Q_{1,\phi}$, we can deduce that $Q_{1,\phi} \geq 0$ for all γ , indicating that the F_1 quadrature of initial PCS $|\phi\rangle$ never exhibits squeezing. Furthermore, if the third term, $2Re[\gamma]$, in $Q_{2,\phi}$ exceeds the sum of the first and second terms, its value becomes negative, leading to the possibility of quadrature squeezing in F_2 .

To provide a clearer analysis of quadrature squeezing, we rely on numerical calculations, with the results presented in Figs. 2 and 3. In Fig. 2, we plot $Q_{1,\Psi}$ as a function of the parameter γ for various coupling strength parameters Γ , while the weak value $\langle \sigma_x \rangle_w = 5.671$ is fixed, corresponding to $\alpha = 8\pi/9$. As shown in Fig. 2, $Q_{1,\phi}$ ($\Gamma = 0$) remains positive and increases with γ [see the thick green curve]. Additionally, Fig. 2 demonstrates that $Q_{1,\Psi}$ for cases where $\Gamma \neq 0$ also consistently takes positive values. This observation confirms that after the postselected von Neumann measurement, the F_1 quadrature of the enhanced PCS $|\Psi\rangle$ still doesn't exhibit squeezing, consistent with the behavior of the initial state.

In Fig. 3, we present the numerical results for $Q_{2,\Psi}$, which corresponds to the quadrature F_2 of the enhanced PCS $|\Psi\rangle$. In Fig. 3(a), $Q_{2,\Psi}$ is plotted as a function of the parameter γ for various coupling strength parameters Γ , with a fixed large weak value $\langle \sigma_x \rangle_w = 5.671$, corresponding to $\alpha = 8\pi/9$. Among these curves, the case $\Gamma = 0$ (thick green curve) represents $Q_{2,\phi}$ for the initial state. As shown, $Q_{2,\phi}$ decreases with increasing γ and converges to -0.125 across most parameter regions. Experimentally, the amount of squeezing is quantified in terms of decibels (dB) [58]. This value of -0.125 corresponds to 9 dB or 50% squeezing. Notably, in the specific case where the PND is $\delta = 0$, $Q_{2,\phi}$ is consistently less

than zero. Thus, the initial PCS $|\phi\rangle$ with $\delta = 0$ always exhibits squeezing along the F_2 quadrature.

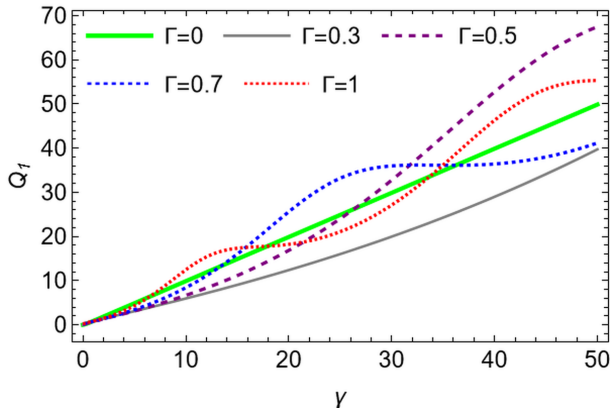


Figure 2. Quadrature squeezing $Q_{1,\Psi}$ as a function of the parameter γ . The thick green line corresponds to the interaction parameter $\Gamma = 0$, representing the case where the state is the initial PCS $|\phi\rangle$. The solid gray line represents $\Gamma = 0.3$, while the purple, blue, and red dashed lines correspond to $\Gamma = 0.5$, $\Gamma = 0.7$, and $\Gamma = 1$, respectively. For these calculations, we take $\delta = 0$, $\alpha = \frac{8\pi}{9}$ and $\varphi = 0$.

In Fig. 3(a), after the postselected von Neumann measurements ($\Gamma \neq 0$), we observe that the value of $Q_{2,\Psi}$ is lower than $Q_{1,\phi}$ for the weak interaction parameter $\Gamma = 0.3$. This behavior persists over a larger range of the parameter γ , indicating that the squeezing characteristics of the quadrature F_2 are enhanced under postselected von Neumann measurements. However, as the interaction coupling strength parameter Γ increases, the value of $Q_{2,\Psi}$ decreases further compared to the $\Gamma = 0.3$ case. For $\Gamma = 0.3$, the minimum value of $Q_{2,\Psi}$ reaches approximately -0.172 near $\gamma = 10$. This corresponds to a squeezing level of 11dB or 69%. Therefore, after performing postselected WMs, the quadrature squeezing along the F_2 direction of the field increases by approximately 19% under suitable system parameters and weak values of the measured system observable. To further investigate the signal amplification effect of weak values for weak system signals, Fig. 3(b) presents $Q_{2,\Psi}$ as a function of the weak value angle α for different coupling strength parameters Γ and a fixed $\gamma = 10$. The numerical results in Fig. 3(b) indicate that the weak value amplifies the squeezing effects of $Q_{2,\Psi}$ when the interaction coupling strength parameter Γ is small, highlighting the signal amplification capability of weak measurements. These results demonstrate that the squeezing effects of $Q_{2,\Psi}$ can be enhanced by postselected WMs.

B. Sum squeezing

The sum squeezing (SQ), a higher-order of squeezing, can also characterize the nonclassicality of a two-mode radiation field. The concept of two-mode SQ for a ra-

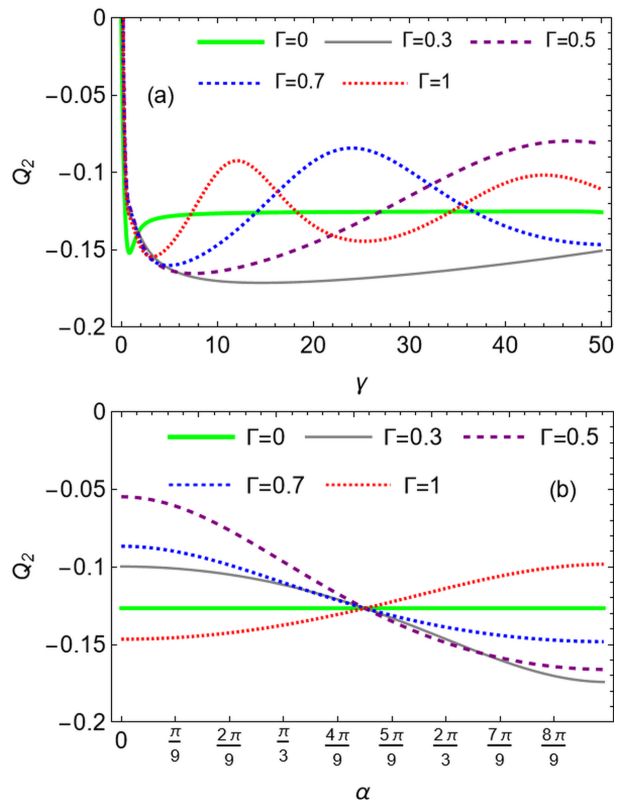


Figure 3. Quadrature squeezing $Q_{2,\Psi}$: (a) $Q_{2,\Psi}$ as a function of the parameter γ for different coupling strength parameters Γ , with the weak value fixed at $\langle\sigma_x\rangle_w = 5.671$ corresponding to $\alpha = 8\pi/9$. (b) $Q_{2,\Psi}$ as a function of the weak value parameter α for different coupling strength parameters Γ , with the parameter γ fixed at 10. Other parameters are the same as those in Fig. 2.

diation field was introduced by Hillery [59]. The sum squeezing operator is defined as:

$$V_\varpi = \frac{1}{2} (e^{i\varpi} a^\dagger b^\dagger + e^{-i\varpi} ab), \quad (24)$$

where the angle $\varpi \in [0, 2\pi]$. Similar to single-mode squeezing, the SQ degree $S_{ab}(\varpi)$ of a two-mode radiation field is defined as

$$S_{ab}(\varpi) = \frac{4\langle(\Delta V_\varpi)^2\rangle}{\langle N_a + N_b + 1\rangle} - 1, \quad (25)$$

where $\Delta V_\varpi^2 = \langle V_\varpi^2 \rangle - \langle V_\varpi \rangle^2$, and particle number operators for the a -mode and b -mode are $N_a = a^\dagger a$ and $N_b = b^\dagger b$, respectively. If $-1 \leq S_{ab}(\varpi) < 0$, the two-mode state exhibits squeezing properties. The more negative the value of $S_{ab}(\varpi)$, the greater the degree of sum squeezing in the state. The state is maximally squeezed when $S_{ab}(\varpi) = -1$. By substituting V_ϖ into Eq. (25), we obtain the squeezing degree $S_{ab}(\varpi)$ of

normal-ordering operators:

$$S_{ab}(\varpi) = \frac{2 \left[\text{Re}[e^{-2i\varpi} \langle a^2 b^2 \rangle] - 2 \left(\text{Re}[e^{-i\varpi} \langle ab \rangle] \right)^2 + \langle N_a N_b \rangle \right]}{\langle N_a \rangle + \langle N_b \rangle + 1} \quad (26)$$

The explicit expression of the SQ degree $S_{ab,\Psi}(\varpi)$ for the enhanced state $|\Psi\rangle$ can be derived by substituting the relevant expectation values, as listed in Appendix A. When $\Gamma = 0$, no measurements is performed, and the state remains as the initial PCS $|\phi\rangle$. For this trivial case, it is straightforward to verify that the sum squeezing equals to zero, i.e., $S_{ab,\phi}(\varpi) = 0$. This result implies that, regardless of the PND δ of the two-modes or the angle ϖ , the SQ of the initial PCS $|\phi\rangle$ is always zero.

In Fig. 4, we present the SQ degree $S_{ab,\Psi}(\varpi)$ for the enhanced PCS $|\Psi\rangle$. In Fig. 4(a), we show $S_{ab,\Psi}(\varpi)$ as a function of the parameter γ for different values of the coupling strength parameter Γ , while fixing the weak value to $\langle \sigma_x \rangle_w = 5.671$, which corresponds to $\alpha = 8\pi/9$. As shown in Fig. 4(a), SQ occurs in a small range of the parameter γ for appropriate coupling strengths Γ , provided the weak value of the measured system observable is large. For the anomalous weak value $\langle \sigma_x \rangle_w = 5.671$, that corresponds to $\alpha = 8\pi/9$, the minimum value of SQ degree $S_{ab,\Psi}(\varpi)$ occurs near $\gamma = 0.5$ at larger interaction strengths Γ . This squeezing effect diminishes as γ increases beyond this range. To further investigate the dependence of SQ on the weak value, Fig. 4(b) presents the variation $S_{ab,\Psi}(\varpi)$ as a function of the weak value parameter α for different values of Γ , while keeping $\gamma = 0.5$ fixed. As indicated in Fig. 4(b), the SQ degree $S_{ab,\Psi}(\varpi)$ takes negative values only for anomalous weak values and non-zero interaction strengths Γ . Notably, when the weak value angle α approaches π , the SQ effect becomes more pronounced for suitable Γ . This numerical result further confirms the amplification effect of weak values in postselected WMs within our scheme.

In the above discussions, we can conclude that the postselected von Neumann measurement improves various squeezing characteristics of our initial PCS $|\phi\rangle$. That is to say, after postselected von Neumann measurement, the squeezing effects of $|\phi\rangle$ are enhanced for large anomalous weak values of the measured observable, with proper composite system parameters γ and Γ . Besides the squeezing effect, quantum correlation functions and entanglement, which exist between the two modes, also characterize the nature of the PCS $|\phi\rangle$. In the next sections, we investigate the effects of the postselected von Neumann measurement on the quantum correlation functions and entanglement features of the PCS $|\phi\rangle$.

IV. THE EFFECTS ON QUANTUM CORRELATION FUNCTIONS

To examine the effects of postselected von-Neumann measurement on the SOCC function $g_{ab}^{(2)}$ of the PCS, in

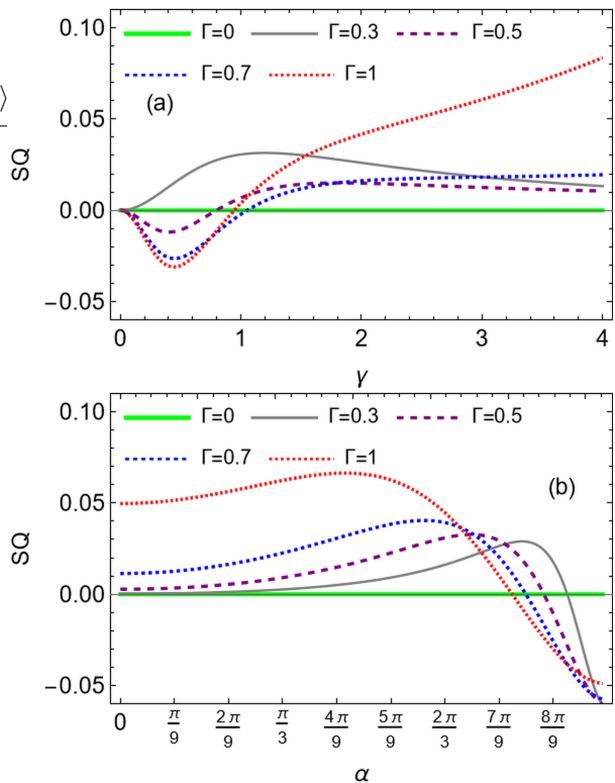


Figure 4. The SQ of our enhanced PCS $|\Psi\rangle$ after postselected von Neumann measurement. (a) $S_{ab,\Psi}(\varpi)$ as a function of the parameter γ for different coupling strength parameters Γ , while the weak value is fixed to $\langle \sigma_x \rangle_w = 5.671$. (b) $S_{ab,\Psi}(\varpi)$ as a function of the weak value parameter α for different coupling strength parameters Γ , while the parameter γ is fixed at 0.5. Here, we take $\varpi = 0$. Other parameters are the same as in Fig. 2.

this section, we investigate the correlation functions between the two modes.

A. Second-order cross-correlation function

The normalized SOCC of the two-mode field is defined as [60]

$$g_{ab}^{(2)} = \frac{\langle a^\dagger a b^\dagger b \rangle}{\langle a^\dagger a \rangle \langle b^\dagger b \rangle}. \quad (27)$$

Here, $\langle a^\dagger a b^\dagger b \rangle$ represents the intensity-intensity correlation between the two-modes, and $\langle a^\dagger a \rangle$ and $\langle b^\dagger b \rangle$ denote mean photon number for each mode, respectively. This function characterizes the correlation between photons in the different modes. If $g_{a,b,\Psi}^{(2)} > 1$, there is correlation between the a -mode and b -mode of the two-mode radiation field. Otherwise, they are inversely correlated. To discuss the properties of $g_{a,b,\Psi}^{(2)}$, we first derive the average values of $\langle a^\dagger a b^\dagger b \rangle$, $\langle a^\dagger a \rangle$, and $\langle b^\dagger b \rangle$ under the state $|\Psi\rangle$. Since their explicit expressions are cumbersome, we

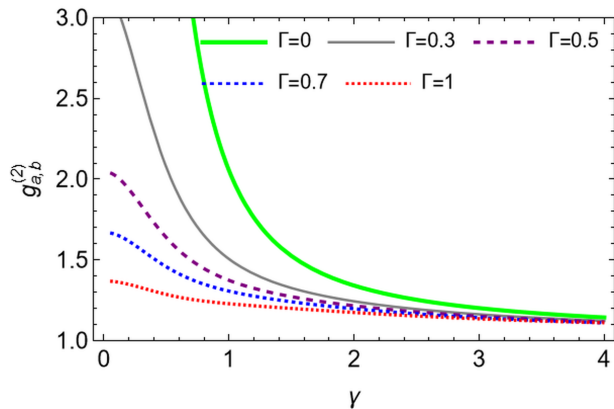


Figure 5. SOCC $g_{ab,\Psi}^{(2)}(0)$ as a function of the state parameter γ for different coupling strength parameters Γ . The green thick curve corresponds to the initial $|\phi\rangle$ case ($\Gamma = 0$). Here, we take weak value as $\langle\sigma_x\rangle_w = 5.761$ and the other parameters are the same as in Fig. 2.

list them in Appendix A. In particular, when $\Gamma = 0$, the SOCC $g_{ab,\Psi}^{(2)}$ reduces to $g_{ab,\phi}^{(2)}$ for the initial PCS $|\phi\rangle$, and its expression can be written as

$$g_{ab,\phi}^{(2)} = \frac{I_\delta(2|\gamma|)^2}{I_{\delta-1}(2|\gamma|)I_{\delta+1}(2|\gamma|)}. \quad (28)$$

As investigated in previous studies [20, 44], the cross-correlation function $g_{ab,\phi}^{(2)}$ between the a -mode and the b -mode of the PCS $|\phi\rangle$ decreases as the PND δ and the parameter γ increase, and eventually, $g_{ab,\phi}^{(2)}$ tends to a value of 1, indicating that the correlation between the two modes is almost non-existent.

In Fig. 5 shows the variation of $g_{ab,\Psi}^{(2)}$ for different system parameters. Specifically, in Fig. 5, we plot $g_{a,b,\Psi}^{(2)}$ as a function of the parameter γ for different coupling strength parameters Γ , while fixing the weak value to $\langle\sigma_x\rangle_w = 5.761$. As shown in Fig. 5, the SOCC $g_{ab,\Psi}^{(2)}$ of the state $|\Psi\rangle$ decreases as the coupling strength parameter Γ increases. When the parameter γ is small, the value of $g_{ab,\Psi}^{(2)}(0)$ is greater than one. However, as γ increases, all curves tend to one. The higher the interaction parameter Γ , the lower the correlation between the two modes of our enhanced PCS $|\Psi\rangle$.

B. second-order correlation function

We can examine the statistical properties of the radiation field by using the zero-time delay second-order correlation function $g^{(2)}(0)$. This function measures the intensity correlation and serves as a crucial parameter for characterizing the photon statistics of a source. For a coherent source, $g^{(2)}(0) = 1$, and for a single-photon state $g^{(2)}(0) = 0$ [61]. If $0 \leq g^{(2)}(0) < 1$, the field exhibits sub-Poissonian statistics, characterizing the non-classical fea-

tures of the associated radiation field [58]. For our state $|\Psi\rangle$, the function $g^{(2)}(0)$ for each mode can be written as:

$$g_a^{(2)} = \frac{\langle a^{\dagger 2} a^2 \rangle}{\langle a^\dagger a \rangle^2}, \quad (29)$$

$$g_b^{(2)} = \frac{\langle b^{\dagger 2} b^2 \rangle}{\langle b^\dagger b \rangle^2}. \quad (30)$$

We derived the explicit expressions of $g^{(2)}(0)$ by calculating the average values of the associated operators (see Appendix A). Figure 6 displays the variations of $g_{a,\Psi}^{(2)}(0)$ and $g_{b,\Psi}^{(2)}(0)$ with the state parameter γ for different coupling strength parameters Γ . We fixed the weak value parameter at $\alpha = 8\pi/9$ to analyze the effects of large anomalous weak values on the statistical properties of our enhanced state $|\Psi\rangle$. As shown in Fig. 6, the $\Gamma = 0$ case corresponds to the $g^{(2)}(0)$ of the initial PCS state $|\phi\rangle$. Its value for both a and b -modes is smaller than one and approaches one as the parameter γ increases (see green curves in Figs. 6(a) and 6(b)). After the postselected von Neumann measurement ($\Gamma \neq 0$), for small parameter γ , the values of the second-order correlation functions $g_a^{(2)}(0)$ and $g_b^{(2)}(0)$ quickly reach their minimum values with increasing coupling strength parameter Γ , similar to the single-photon state case. On the other hand, for large values of the state parameter ($\gamma \gg 1$), $g_a^{(2)}(0)$ and $g_b^{(2)}(0)$ become indistinguishable for all coupling strength parameters Γ and tend to one, which corresponds to the coherent state case. This result also explains why the SOCC $g_{ab,\Psi}^{(2)}$ of $|\Psi\rangle$ approaches one when $\gamma \gg 1$ (see Fig. 5).

It is interesting to note that when comparing the green thick curve ($\Gamma = 0$) with other curves in Figs. 6(a) and 6(b), the second-order correlation function of the a -mode and b -mode changes more dramatically after the postselected measurement ($\Gamma \neq 0$). Due to the weak value amplification effects, this result allows us to achieve the characteristics of a single-photon state in small regions of the state parameter γ . Our numerical results suggest that following the postselected von Neumann measurement, the two modes of our enhanced output state $|\Psi\rangle$ could potentially generate a single-photon field [62, 63].

V. THE EFFECTS ON ENTANGLEMENT

In this section, we investigate the effects of postselected von Neumann measurement on quantum correlations of the PCS. In a previous study [64], the inseparability of the PCS were confirmed in light of the Peres-Horodecki criterion and various entropies. Here, we separately examine the HZ correlation and EPR correlation to analyze the inseparability of our enhanced output state $|\Psi\rangle$, as defined in Eq. (10).

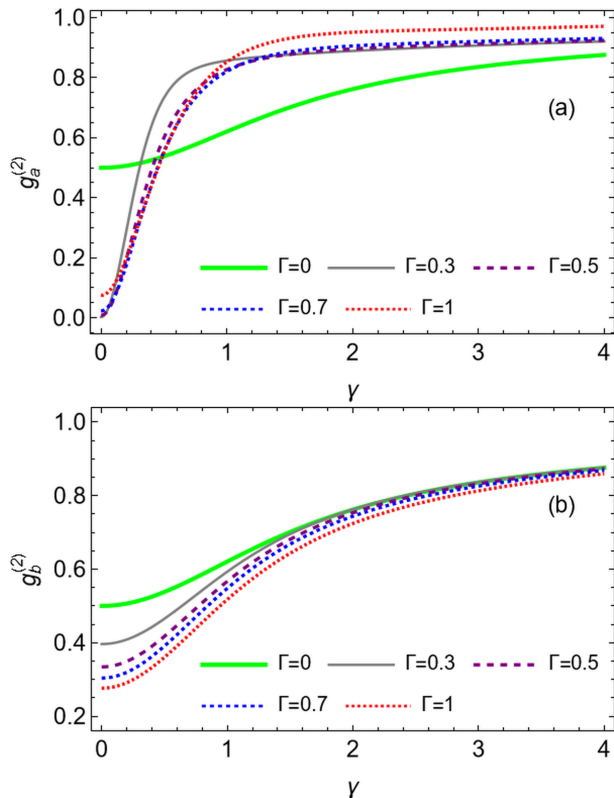


Figure 6. Second-order correlation as a function of the a and b -modes of the state $|\Psi\rangle$. (a) $g_{a,\Psi}^{(2)}(0)$ as a function of the state parameter γ for different coupling strength parameters Γ for mode a . (b) the b mode's $g_{b,\Psi}^{(2)}(0)$ as a function of the state parameter γ for different coupling strength parameters Γ . Here, we take weak value as $\langle\sigma_x\rangle_w = 5.761$ and other parameters are the same as in Fig. 2.

A. HZ correlation

First, we study the entanglement between the two modes in the light field by adopting the inequality provided by Hillery and Zubairy [65]. This is defined as [7]:

$$E = \langle N_a \rangle \langle N_b \rangle - |\langle ab \rangle|^2. \quad (31)$$

If $E < 0$, it implies that the state exhibits entanglement between the two modes. From the CSI, $|\langle ab \rangle|^2 \leq \langle a^\dagger a \rangle \langle b^\dagger b \rangle$ [66], the entanglement condition for two-mode fields is bounded as $-\langle N_a \rangle \leq E < 0$. It is straightforward to verify that the HZ correlation function E for the initial PCS $|\phi\rangle$ can be expressed as:

$$\begin{aligned} E_\phi &= \frac{|\gamma|^2 I_{\delta-1}(2|\gamma|) I_{\delta+1}(2|\gamma|)}{I_\delta(2|\gamma|)^2} - |\gamma|^2 \\ &= |\gamma|^2 \left(\frac{1}{g_{ab,\phi}^{(2)}} - 1 \right), \end{aligned} \quad (32)$$

where $g_{ab,\phi}^{(2)}$ is the SOCC defined in Eq. 28. To evaluate the HZ correlation for our output state $|\Psi\rangle$, we compute

E_Ψ using Eq. (31), substituting the average values of $\langle ab \rangle$, $\langle a^\dagger a \rangle$ and $\langle b^\dagger b \rangle$ as listed in Appendix A. To demonstrate the effects of postselected von Neumann measurement on the entanglement of the output state $|\Psi\rangle$, we introduce the difference between E_Ψ and E_ϕ , defined as $\Delta E = E_\Psi - E_\phi$. Fig. 7 presents the numerical results for ΔE . If $\Delta E < 0$, it indicates that the degree of entanglement has increased compared to the initial state; otherwise, it has decreased. In Fig. 7(a), ΔE is plotted as a function of the state parameter γ for different values of PND denoted by δ , with the coupling strength parameter Γ fixed in the WM regime ($\Gamma = 0.3$) and a large anomalous weak value $\langle\sigma_x\rangle_w = 5.761$. The results show that ΔE takes negative values for certain regions of γ , and these regions expand as δ increases. This result indicates that the final MD $|\Psi\rangle$ exhibits stronger entangled properties than the initial PCS $|\phi\rangle$ in appropriate parameter regions. To further validate the role of weak value amplification for enhancing the entanglement between two modes of PCS after postselected measurement, Fig. 7(b) illustrates the variation of ΔE with the weak value parameter α for different values of δ . The curves in Fig. 7(b) reveal that, within the WM regime, if the PND δ between modes a and b of the PCS is equal to or greater than two (i.e., $\delta \geq 2$), the entanglement between the two modes of the measurement output state $|\Psi\rangle$ surpasses that of the initial state $|\phi\rangle$ for large anomalous weak values.

B. EPRs correlation

Another inseparability criterion for two-mode systems in multimode continuous variable systems relies on the total variance of a pair of EPR-type operators [67]. This criterion provides a sufficient condition for entanglement in any two-party continuous variable state and is also a necessary and sufficient condition for inseparability. For a two-mode system, the EPR correlation is defined in terms of the variances of the EPR-type operators $X_1 - X_2$ and $P_1 - P_2$ as [68]

$$\begin{aligned} I &= \langle \Delta^2 (X_1 - X_2) \rangle + \langle \Delta^2 (P_1 - P_2) \rangle \\ &= 2(1 + \langle a^\dagger a \rangle + \langle b^\dagger b \rangle - \langle a^\dagger b^\dagger \rangle - \langle ab \rangle) \\ &\quad - 2(\langle a \rangle - \langle b^\dagger \rangle)(\langle a^\dagger \rangle - \langle b \rangle). \end{aligned} \quad (33)$$

where $X_1 = \frac{a+a^\dagger}{\sqrt{2}}$, $X_2 = \frac{b+b^\dagger}{\sqrt{2}}$, $P_1 = \frac{a-a^\dagger}{i\sqrt{2}}$ and $P_2 = \frac{b-b^\dagger}{i\sqrt{2}}$. If the total variance is less than 2, $I < 2$, the two-mode system can be considered inseparable, indicating quantum entanglement. Otherwise, the system is classical. The smaller the value of I , the stronger the EPR correlation.

The explicit expression of the EPR correlation I_Ψ of our postselected measurement output state $|\Psi\rangle$ can be obtained by substituting the associated averages listed in Appendix A into Eq. (33). As a special case, when

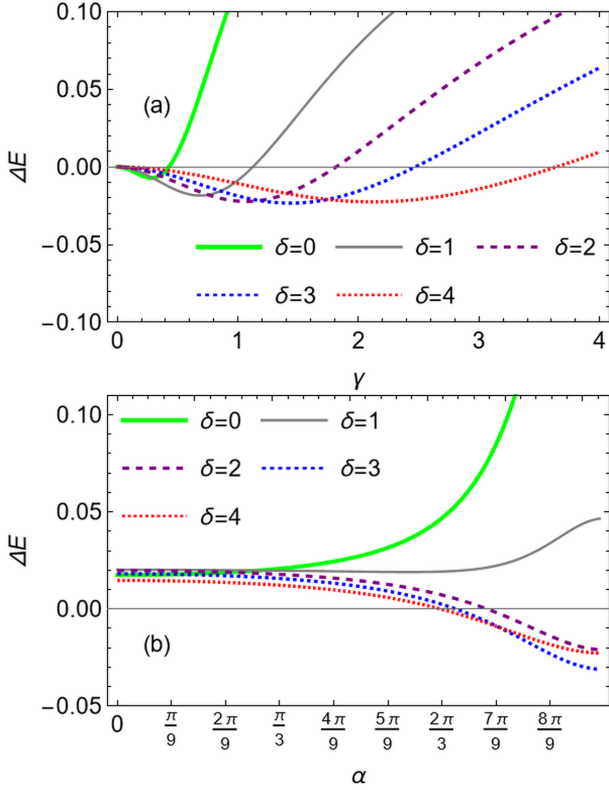


Figure 7. HZ correlation between two modes of the state $|\Psi\rangle$. (a) ΔE as a function of the state parameter γ for different PND values δ , with $\langle\sigma_x\rangle_w = 5.761$. (b) ΔE as a function of the weak value parameter α for different PND values δ , with $\gamma = 1.5$. Here, we take $\Gamma = 0.3$ and other parameters are the same as in Fig. 2.

$\Gamma = 0$, I_Ψ reduces to the EPR correlation I_ϕ of the initial PCS $|\phi\rangle$, and its expression reads as

$$I_\phi = 2 \left(\frac{|\gamma|I_{\delta-1}(2|\gamma|)}{I_\delta(2|\gamma|)} + \frac{|\gamma|I_{\delta+1}(2|\gamma|)}{I_\delta(2|\gamma|)} - 2\Re(\gamma) + 1 \right) = 8Q_{2,\phi} + 2 = 8\Delta F_{2,\phi}^2. \quad (34)$$

Here, $Q_{2,\phi}$ is the quadrature squeezing parameter of the initial PCS $|\phi\rangle$ as defined in Eq. (23), and $\Delta F_{2,\phi}^2$ represents the variance of the quadrature operator $F_{2,\phi}$, defined in Eq. (17), over the state $|\phi\rangle$. For the PCS state $|\phi\rangle$, its EPR correlation is proportional to the variance $\Delta F_{2,\phi}^2$. To analyze the effects of the postselected von Neumann measurement on the EPR correlation between the two modes of the state $|\Psi\rangle$, we introduce the difference between I_Ψ and I_ϕ , defined as $\Delta I = I_\Psi - I_\phi$. To observe these effects, we plotted ΔI as a function of various system parameters, with the numerical results shown in Fig. 8. The variation of ΔI with changes in the state parameter γ for different PND δ is presented in Fig. 8(a). When the weak value is set to $\langle\sigma_x\rangle_w = 5.761$ and the coupling strength parameter is fixed at $\Gamma = 0.3$, ΔI takes negative values in a range of the state parameter γ for cases where $\delta \geq 2$. The regions of negative values become broader

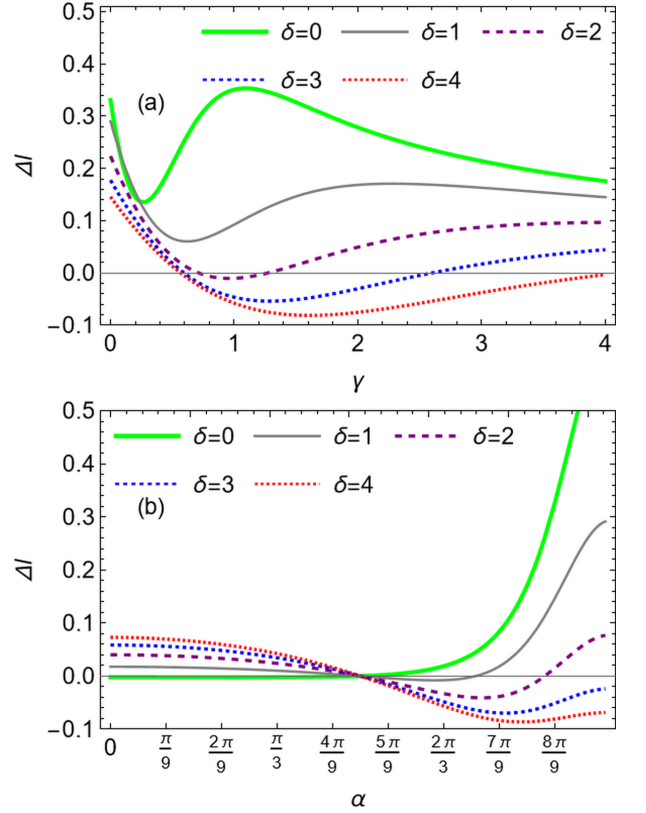


Figure 8. EPR correlation differences ΔI for the states $|\Psi\rangle$ and $|\phi\rangle$. (a) ΔI as a function of the state parameter γ for different PND δ between the two modes of the state $|\Psi\rangle$. (b) ΔI as a function of the weak value angle α for different PND δ between the two modes of the state $|\phi\rangle$. Here $\Gamma = 0.3$, with (a) $\langle\sigma_x\rangle_w = 5.761$, and (b) $\gamma = 1.5$. Other parameters are the same as in Fig. 2.

and deeper as the PND δ between the two modes increases. This result implies that in the postselected WM regime ($\Gamma \ll 1$) with large anomalous weak values, the EPR correlation between the two modes of the state $|\Psi\rangle$ is stronger than that of the initial PCS state $|\phi\rangle$ when $\delta \geq 2$. Similar to the HZ correlation case, we examined the dependence of the enhancement of the entanglement on the anomalous weak values. Fig. 8(b) shows ΔI as a function of the angle α . The curves in Fig. 8(b) show that larger PND δ does not enhance the violation of the EPR correlation for small weak value angles α . However, for larger weak value angles α , ΔI becomes negative, and its absolute value increases with increasing PND δ .

In summary, the large anomalous weak values $\langle\sigma_x\rangle_w$ of the measured system observable contribute significantly to the weak signal amplification observed in our scheme.

VI. JOINT WIGNER FUNCTION

To gain a deeper understanding of the effects of post-selected von Neumann measurements on the properties

of $|\Psi\rangle$, we examine the phase space distribution by calculating its Wigner function. The Wigner function of a single-mode radiation field can be written as [58]:

$$W(\alpha) = \frac{2}{\pi} \text{Tr} [\rho D(\alpha) P D^\dagger(\alpha)], \quad (35)$$

where ρ is the density operator of the given state, and P is the parity operator. However, in our current work, this Wigner function cannot be used directly since the PCS is a two-mode radiation field. In the two-mode case, the Wigner function of our state $|\Psi\rangle$ can be expressed in terms of the joint Wigner function

$$\begin{aligned} W_J(\alpha, \beta) &= \frac{4}{\pi^2} \text{Tr} [\rho D(\alpha) D(\beta) P_j D^\dagger(\beta) D^\dagger(\alpha)] \\ &= \frac{4}{\pi^2} P_J(\alpha, \beta), \end{aligned} \quad (36)$$

where $\rho = |\Psi\rangle\langle\Psi|$ is the density operator of the state $|\Psi\rangle$, $P_j = P_a P_b = e^{i\pi a^\dagger a} e^{i\pi b^\dagger b}$ is the joint photon number parity operator, and $D(\alpha) = e^{\alpha a^\dagger - \alpha^* a}$ and $D(\beta) = e^{\beta b^\dagger - \beta^* b}$ are the displacement operators acting on the a and b modes of the two-mode state $|\Psi\rangle$, respectively. The joint Wigner function W_J is a function in the 4D phase space, whose coordinates are $(\text{Re}(\alpha), \text{Im}(\alpha), \text{Re}(\beta), \text{Im}(\beta))$. In Eq. (36), $P_J(\alpha, \beta)$ is referred to as the scaled Wigner function, which we use for our analysis of the phase space distribution of the measurement output state $|\Psi\rangle$. Upon examining the expression for $P_J(a, \beta)$, we find that it is the average value of the joint parity operator P_j after applying displacement operators with amplitudes $-\alpha$ and $-\beta$ to the a and b modes, respectively. Since the eigenstates of the parity operators P_a and P_b are the Fock states $|n\rangle_a$ and $|n\rangle_b$, with eigenvalues $(-1)^{n_a}$ and $(-1)^{n_b}$, the scaled Wigner function is therefore bounded by ± 1 , i.e.,

$$-1 \leq P_J(\alpha, \beta) \leq 1. \quad (37)$$

To illustrate the core features in this 4D Wigner function of the state $|\Psi\rangle$ and compare it with the initial PCS state $|\phi\rangle$, we first present the 2D cuts along the $\text{Re}(\alpha) - \text{Re}(\beta)$ plane and the $\text{Im}(\alpha) - \text{Im}(\beta)$ plane of the joint Wigner function of $|\phi\rangle$, as shown in Fig. 9. Figs. 9(a) and 9(b) represent the density plot of the joint Wigner function of the initial PCS state $|\phi\rangle$ with $\gamma = 0.5$ and $\delta = 0$, in the planes $\text{Im}(\alpha) = \text{Im}(\beta) = 0$ and $\text{Re}(\alpha) = \text{Re}(\beta) = 0$, respectively. As shown in these figures, the initial PCS $|\phi\rangle$ is Gaussian when there is no PND between the two modes ($\delta = 0$), and it exhibits squeezing along the F_2 quadrature (see Sec. III A). Similarly, Figs. 9(c) and 9(d) show the density plots of the joint Wigner function of the initial PCS state $|\phi\rangle$ with $\gamma = 0.5$ and $\delta = 2$, in the planes $\text{Im}(\alpha) = \text{Im}(\beta) = 0$ and $\text{Re}(\alpha) = \text{Re}(\beta) = 0$, respectively. It is evident that when there is PND between the two modes ($\delta = 2$), the state $|\phi\rangle$ becomes non-Gaussian. Additionally, the characteristic interference fringes of the PCS are visible, indicating substantial coherence and consistent multiphoton

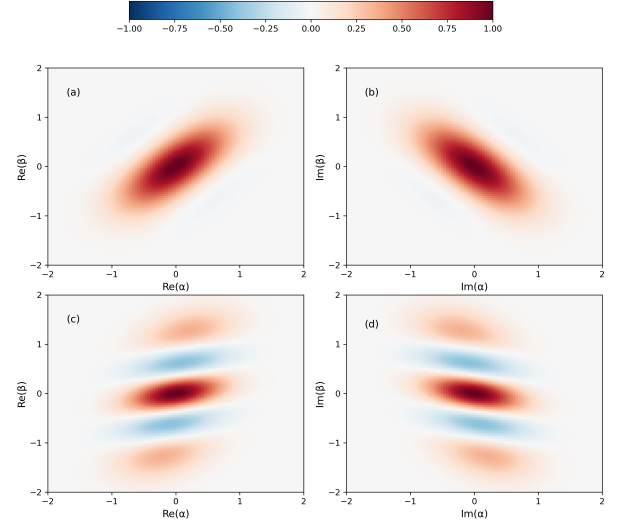


Figure 9. Cuts in the scaled two-mode Wigner function. (a and b) A 2D plane cut along (a) the $\text{Re}(\alpha) - \text{Re}(\beta)$ axes and (b) $\text{Im}(\alpha) - \text{Im}(\beta)$ axes of the calculated 4D scaled joint Wigner function $P_J(\alpha, \beta)$ for the initial PCS state $|\phi\rangle$ with $\delta = 0$. (c and d) A 2D plane cut along (c) the $\text{Re}(\alpha) - \text{Re}(\beta)$ axes and (d) the $\text{Im}(\alpha) - \text{Im}(\beta)$ axes of the calculated 4D scaled joint Wigner function $P_J(\alpha, \beta)$ of the initial PCS state $|\phi\rangle$ with $\delta = 2$. Here, $\gamma = 0.5$.

phases. This result suggests that PND ($\delta \neq 0$) between the two modes is crucial for enhancing the nonclassicality of the PCS state $|\phi\rangle$.

In Fig. 10, we present the scaled joint Wigner function $P_J(\alpha, \beta)$ of the state $|\Psi\rangle$ with $\Gamma = 0.3$, $\gamma = 0.5$, $\langle\sigma_x\rangle_w = 5.761$, and $\delta = 2$. We observe that this Wigner function exhibits highly nonclassical characteristics in phase space. Compared to the initial PCS state $|\phi\rangle$ (see Figs. 9(c) and 9(d)), we can see that after the postselected measurement, the shapes of the scaled joint Wigner functions not only show good squeezing for the appropriate coupling strength parameter Γ and large anomalous weak value $\langle\sigma_x\rangle_w$, but we also can observe clear quantum interference structures formed between the peaks (see Figs. 10(c) and 10(d)). Furthermore, if someone take comparison Fig. 9 and Fig. 10 who can find that after postselected von Neumann measurement the negative values of Wigner function increased for large anomalous weak value compared to initial state case. This indicated that the nonclassicality of the PCS enhanced after the postselected von Neumann measurement.

These phase space analyses demonstrate that after the postselected von Neumann measurement, the nonclassicality and non-Gaussianity of our PCS state $|\phi\rangle$ enhanced due to the weak signal amplification feature of the weak value.

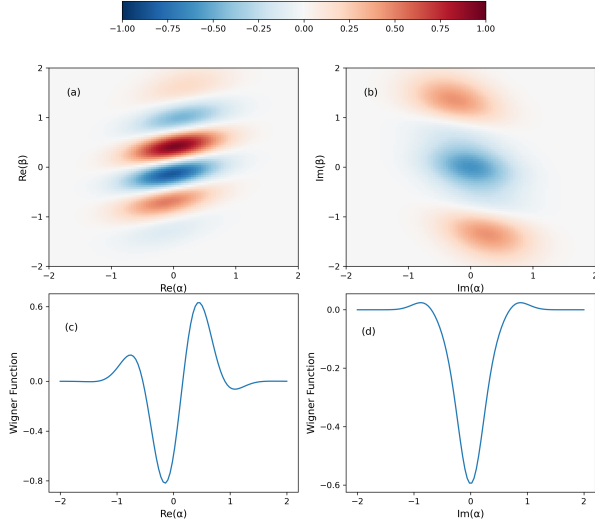


Figure 10. Joint Wigner function of the enhanced PCS state $|\Psi\rangle$ after postselected measurement. (a and b) A 2D plane cut along (a) the $Re(\alpha) - Re(\beta)$ axes and (b) the $Im(\alpha) - Im(\beta)$ axes of the calculated 4D scaled joint Wigner function $P_J(\alpha, \beta)$ for the measurement output state $|\Psi\rangle$ with $\Gamma = 0.3$, $\gamma = 0.5$, $\langle\sigma_x\rangle_w = 5.761$ and $\delta = 2$. (c) Diagonal line cuts of the data shown in (a), corresponding to a 1D plot of the calculated scaled joint Wigner function $P_J(\alpha, \beta)$ along $Re(\alpha) = Re(\beta)$ with $Im(\alpha) = Im(\beta) = 0$. (d) Diagonal line cuts of the data shown in (b), corresponding to a 1D plot of the calculated scaled joint Wigner function $P_J(\alpha, \beta)$ along $Im(\alpha) = Im(\beta)$ with $Re(\alpha) = Re(\beta) = 0$.

VII. FIDELITY

In this section, we examine the state distance between the initial PCS and final MD states, specifically $|\phi\rangle$ and $|\Psi\rangle$ using the fidelity function. The fidelity F is defined as the square of the absolute value of their scalar product, and it is bounded as $0 \leq F \leq 1$, where the lower (higher) boundary represents completely different (identical) states. We define the fidelity function between $|\phi\rangle$ and $|\Psi\rangle$ as:

$$F = |\langle\phi|\Psi\rangle|^2. \quad (38)$$

After substituting $|\phi\rangle$ and $|\Psi\rangle$ (see Eqs. (1) and (10)) into the above formula, one can derive an explicit expression for F . However, we only present the numerical analysis of this quantity. As shown in Fig. 11, the postselected von Neumann measurement indeed causes a change in the given state, resulting in a larger state distance between $|\phi\rangle$ and $|\Psi\rangle$, which even transforms it into a distinguishable state with increasing coupling strength parameter Γ and state parameter γ . Larger anomalous weak values have a more significant effect than smaller ones in distinctly transforming between the states.

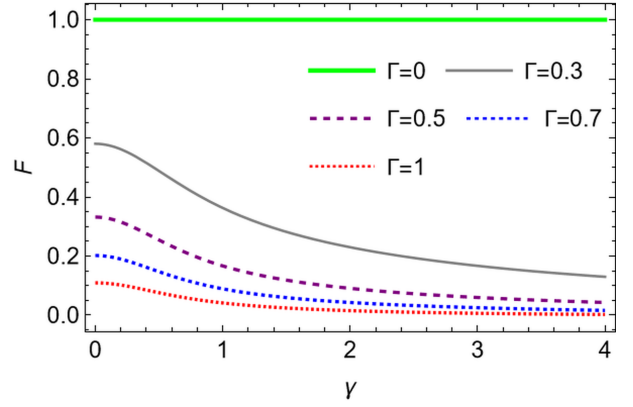


Figure 11. Fidelity F as a function of the state parameter γ . Here, we take weak value as $\langle\sigma_x\rangle_w = 5.761$ and other parameters are the same as Fig. 2.

VIII. DISCUSSION

From the fidelity analysis of our measurement output, the enhanced state $|\Psi\rangle$, we can deduce that after the postselected von Neumann measurement, the initial PCS $|\phi\rangle$ undergoes a dramatic change, potentially transforming into a completely different state. As previous related studies have shown, the postselected von Neumann measurement technique provides an alternative approach to state optimization problems [41]. In this context, we explore the concrete changes and potential applications of our enhanced state $|\Psi\rangle$ in state preparation processes. Depending on the coupling strength parameter Γ and the state parameter γ , we outline its usefulness in the following four scenarios:

(1) Arbitrary values for the state parameter γ and the coupling strength parameter Γ . In this general case, our final state is the measurement output state $|\Psi\rangle$ as defined in Eq. (10). For simplicity, the initial PCS $|\phi\rangle$ expressed in the coherent state representation as [44].

$$|\phi\rangle = \mathcal{N}_n e^{i\gamma} \int \frac{d\theta}{2\pi} [(\gamma)^{1/2} e^{i\theta}]^{-\delta} |(\gamma)^{1/2} e^{i\theta}\rangle_a |(\gamma)^{1/2} e^{-i\theta}\rangle_b. \quad (39)$$

Here, $|(\gamma)^{1/2} e^{i\theta}\rangle_a = D(\sqrt{\gamma} e^{i\theta})|0\rangle_a$ and $|(\gamma)^{1/2} e^{-i\theta}\rangle_b = D(\sqrt{\gamma} e^{-i\theta})|0\rangle_b$ denote the coherent states corresponding to the a and b modes of PCS. In this case, we can rewrite the $|\Psi\rangle$ as the following from

$$|\Psi_1\rangle = \frac{\lambda}{2} \left[t_+ |\gamma + \frac{\Gamma_a}{2}, \delta\rangle + t_- |\gamma - \frac{\Gamma_a}{2}, \delta\rangle \right]. \quad (40)$$

Here, $t_{\pm} = 1 \pm \langle\sigma_x\rangle_w$ and the state $|\gamma \pm \frac{\Gamma_a}{2}, \delta\rangle$ represents the displaced PCS (the displacement operator $D(\pm \frac{\Gamma}{2})$ acts only on a mode), and its expression is given by:

$$|\gamma \pm \frac{\Gamma_a}{2}, \delta\rangle = \frac{\mathcal{N}_n e^{|\gamma|}}{2\pi} \int [(\gamma)^{1/2} e^{i\theta}]^{-\delta} e^{\pm \frac{\Gamma}{2} [iIm\{(\gamma)^{1/2} e^{-i\theta}\}^*]} d\theta \quad (41)$$

$$\times |(\gamma)^{1/2} e^{i\theta} \pm \frac{\Gamma}{2}\rangle_a |(\gamma)^{1/2} e^{-i\theta}\rangle_b d\theta.$$

(2) Strong coupling strength parameter ($\Gamma \gg 1$) with small parameter γ ($|\gamma| \ll 1$). Since the state parameter γ is very small, we expand the Eq. (1) up to the first order of γ and ignore higher order terms. In this extreme case, the Eq. (10) changed to:

$$|\Psi'\rangle \approx \frac{\lambda'}{2} \left\{ \left[\left| t'_+ \left| \frac{\Gamma}{2}, \delta \right\rangle_a + t'_- \left| -\frac{\Gamma}{2}, \delta \right\rangle_a \right] |0\rangle_b + \frac{\gamma}{\sqrt{1+\delta}} \left[\left| t'_+ \left| \frac{\Gamma}{2}, 1+\delta \right\rangle_a + t'_- \left| -\frac{\Gamma}{2}, 1+\delta \right\rangle_a \right] |1\rangle_b \right\}, \quad (42)$$

where $\lambda' = \frac{\sqrt{2}\gamma^{\delta/2}}{\sqrt{\delta!}} [1 + |\langle \sigma_x \rangle_c|^2 + (1 - |\langle \sigma_x \rangle_c|^2)P]^{-\frac{1}{2}}$ and $t'_\pm = 1 \pm \langle \sigma_x \rangle_c$. The states $|\pm \frac{\Gamma}{2}, \delta\rangle_a = D(\pm \frac{\Gamma}{2})|\delta\rangle_a$ and $|\pm \frac{\Gamma}{2}, 1+\delta\rangle_a = D(\pm \frac{\Gamma}{2})|1+\delta\rangle_a$ denote the displaced δ and $1+\delta$ photon Fock states of the a -mode, respectively. Here, $\langle \sigma_x \rangle_c$ represents the conditional expectation value of the measured system observable σ_x , which is measured through the postselected strong measurement. For our pre- and post-selected system states $|\psi_i\rangle$ and $|\psi_f\rangle$, as defined in Sec. II, this conditional expectation value is given by $\langle \sigma_x \rangle_c = \cos \vartheta \sin \alpha$ [69]. It can be observed that the state $|\Psi'\rangle$ is entangled state of the a and b -modes, and interesting quantum phenomena in the a -mode can be explored by adjusting the related parameters.

If the expectation value $\langle \sigma_x \rangle_c = 0$, i.e. $\alpha = 0$, $\vartheta = \frac{\pi}{2}$ or $\frac{3\pi}{2}$, the Eq. (42) changed to $|\Psi'\rangle \approx \left(\left| \frac{\Gamma}{2}, \delta \right\rangle_a + \left| -\frac{\Gamma}{2}, \delta \right\rangle_a \right) |0\rangle_b$, with high probability due to the small state parameter γ . In this case, the b -mode is in the vacuum state, and the a -mode is in superposition of displaced Fock state, i.e., $\left| \frac{\Gamma}{2}, \delta \right\rangle_a + \left| -\frac{\Gamma}{2}, \delta \right\rangle_a$. One interesting point is that if the PND between the two modes is zero ($\delta = 0$), the a mode is prepared in even Schrödinger cat state $\left| \frac{\Gamma}{2} \right\rangle_a + \left| -\frac{\Gamma}{2} \right\rangle_a$. Furthermore, if $\langle \sigma_x \rangle_c = 1$, the above state became another entangled state as $\left| \frac{\Gamma}{2}, \delta \right\rangle_a |0\rangle_b + \frac{\gamma}{\sqrt{1+\delta}} \left| \frac{\Gamma}{2}, 1+\delta \right\rangle_a |1\rangle_b$. If we further assume $|\gamma| \ll 1$, then a mode stated in displaced Fock state $D(\frac{\Gamma}{2})|\delta\rangle_a$ meanwhile the b mode in the vacuum state.

(3) Weak coupling strength parameter ($\Gamma \ll 1$) with state parameter γ ($|\gamma| \gg 1$). In this case, since the coupling strength Γ is small, we can perform a first-order Taylor expansion of the associated operators; The displacement operator is approximately $D(\frac{\Gamma}{2}) \approx \mathbb{I} + \frac{\Gamma}{2}(a^\dagger - a)$. Then, the final MD state $|\Psi\rangle$ (Eq. (10)) changes to (unnormalized):

$$|\Psi''\rangle \approx \left[1 + \frac{\Gamma}{2}(a^\dagger - a) Re[\langle \sigma_x \rangle_w] \right] |\phi\rangle, \quad (43)$$

In this case, the state $|\Psi''\rangle$ is in a superposition of the PCS, single-photon-added PCS, and single photon-subtracted PCS. Most of the phenomena observed in our current work arise from this state.

(4) Weak coupling strength parameter ($\Gamma \ll 1$) with small state parameter γ ($|\gamma| \ll 1$). Here, as both the coupling parameter $\Gamma \ll 1$ and γ are very small, we can neglect $\Gamma\gamma^{1+\delta/2}$ and higher-order terms in our system state. In this extreme case, the expression for our output state $|\Psi\rangle$ further changes to (unnormalized):

$$|\Psi'''\rangle \approx \left\{ \left[|\delta\rangle_a + \frac{\Gamma}{2} Re[\langle \sigma_x \rangle_w] \sqrt{\delta+1} |\delta+1\rangle_a - \frac{\Gamma}{2} Re[\langle \sigma_x \rangle_w] \sqrt{\delta} |\delta-1\rangle_a \right] |0\rangle_b + \frac{\gamma}{\sqrt{1+\delta}} |1+\delta\rangle_a |1\rangle_b \right\}. \quad (44)$$

In this regime, the WVA is dominant, and $\Gamma Re[\langle \sigma_x \rangle_w]$ can become a significant quantity compared to γ , especially if the pre and post-selected system states are nearly orthogonal. If we assume the PND equal zero ($\delta = 0$), the a -mode is prepared in a superposition state of $|0\rangle_a$ and $|1\rangle_a$, while the b -mode remains in the vacuum state. Furthermore, under sufficiently large anomalous weak value, it is possible to detect a single photon from the a -mode with higher probability. This feature could be useful in quantum computation processes, as discussed in [70]. More interestingly, in this extreme case, we can also prepare the state $|1+\delta\rangle_a |1\rangle_b$, but with a lower generation probability. For this extreme case, the advantages of our scheme are highlighted by the very small value regimes shown in the numerical results of Figs. 6(a) and 6(b).

We also note that our theoretical scheme can be realized on an optical platform, as the initial system preparation, post-selection of the measured system, and weak coupling between the measured system and MD can all be accomplished in optical labs, as in previous WVA experiments [71, 72]. Furthermore, it may also be possible to implement our scheme in a trapped ion system, as the von Neumann-type interaction Hamiltonian $H_{int} = g\sigma_x \otimes P_x$ can be prepared in two-dimensional harmonic oscillators of trapped ion systems [51, 73–76].

Finally, the postselected von Neumann measurement utilizes the technique of WVA, which enables the PCS to exhibit excellent non-classical properties. The PCS under postselected von Neumann measurement can show improved performance in squeezing, quantum statistics, and entanglement by selecting appropriate parameters. This method may provide a valuable quantum resource for enhancing the efficiency of quantum teleportation and other quantum tasks based on PCS [10, 54, 55].

IX. CONCLUSION

In this paper, we have proposed a theoretical model to enhance the non-Gaussianity and nonclassicality of PCS using postselected von Neumann measurement. We apply a postselected measurement to one mode (the a -mode) of the PCS and investigate related properties, including squeezing, quantum statistics, and entanglement. The results show that after the postselected von Neumann measurement, the associated characteristics of the measurement output state are enhanced in the WM regime with anomalous weak values. Quadrature squeezing achieves better-squeezing effects than the PCS over a wide range of state parameters γ under WM. The sum squeezing effect occurs due to WVA for larger weak values. Numerical results using HZ correlation and EPR correlation also show that the entanglement between the two modes of the postselected measurement-enhanced PCS becomes stronger than the initial state. We confirm these findings by examining the scaled joint Wigner function for different system parameters. We also analyze the changes in the initial state after the measurement process in terms of fidelity and observe that as the coupling strength parameter Γ increases, the initial state $|\phi\rangle$ changes and can even become orthogonal to $|\phi\rangle$. From this perspective, we also discuss the potential applications of our scheme in quantum state preparation processes. We explored the possibility of performing post-

selected von Neumann measurements in multimode radiation fields. For simplicity, we only considered the postselected measurement on one mode of the PCS. It would be interesting to extend this to postselected measurements on both modes of two-mode states, such as the two-mode squeezed vacuum state, to generate interesting states, including entangled superpositions of two coherent states [4]. In future work, it will also be interesting to study the effects of postselected von Neumann measurements on other Gaussian and non-Gaussian multipartite continuous-variable radiation fields [1, 2, 77], as well as their practical applications and implementations in the laboratory.

ACKNOWLEDGMENTS

This work was supported by the National Natural Science Foundation of China (No. 12365005).

Appendix A: Related expression

Here, we derive explicit expressions for the relevant average values associated with our proposed state $|\Psi\rangle$. However, due to their complexity, many of these expressions are too cumbersome to include in the main text. Therefore, we have provided them in this appendix for reference.

$$\begin{aligned}
\langle a^\dagger a \rangle &= \frac{|\lambda|^2}{2} [(1 + |\langle \sigma_x \rangle_w|^2) P_{11} + (1 - |\langle \sigma_x \rangle_w|^2) P_{12}], \\
P_{11} &= \frac{|\gamma| I_{\delta-1}(2|\gamma|)}{I_\delta(2|\gamma|)} + \frac{\Gamma^2}{4}, \\
P_{12} &= \mathcal{N}_n^2 \sum_{n=0}^{\infty} \frac{|\gamma|^{2n+\delta}}{n!(n+\delta-1)!} e^{-\frac{\Gamma^2}{2}} L_{n+\delta}^{(0)}(\Gamma^2) \\
&\quad - \frac{\Gamma}{2} \mathcal{N}_n^2 \sum_{n=0}^{\infty} \frac{|\gamma|^{2n+\delta}}{n!(n+\delta)!} e^{-\frac{\Gamma^2}{2}} \Gamma L_{n+\delta}^{(1)}(\Gamma^2) \\
&\quad + \frac{\Gamma}{2} \mathcal{N}_n^2 \sum_{n=0}^{\infty} \frac{|\gamma|^{2n+\delta}}{n!(n+\delta)!} e^{-\frac{\Gamma^2}{2}} \Gamma L_{n+\delta-1}^{(1)}(\Gamma^2) \\
&\quad + \frac{\Gamma^2}{4} \mathcal{N}_n^2 \sum_{n=0}^{\infty} \frac{|\gamma|^{2n+\delta}}{n!(n+\delta)!} e^{-\frac{\Gamma^2}{2}} L_{n+\delta}^{(0)}(\Gamma^2).
\end{aligned} \tag{A1}$$

$$\begin{aligned}
\langle b^\dagger b \rangle &= \frac{|\lambda|^2}{2} [(1 + |\langle \sigma_x \rangle_w|^2) P_{21} + (1 - |\langle \sigma_x \rangle_w|^2) P_{22}], \\
P_{21} &= \frac{|\gamma| I_{\delta+1}(2|\gamma|)}{I_\delta(2|\gamma|)}, \\
P_{22} &= \mathcal{N}_n^2 \sum_{n=0}^{\infty} \frac{|\gamma|^{2n+\delta}}{(n-1)!(n+\delta)!} e^{-\frac{\Gamma^2}{2}} L_{n+\delta}^{(0)}(\Gamma^2).
\end{aligned} \tag{A2}$$

$$\langle ab \rangle = \frac{|\lambda|^2}{2} [(1 + |\langle \sigma_x \rangle_w|^2) P_{31} + (1 - |\langle \sigma_x \rangle_w|^2) P_{32}], \quad (\text{A3})$$

$$P_{31} = \gamma,$$

$$P_{32} = \mathcal{N}_n \mathcal{N}_{n-1} \sum_{n=0}^{\infty} \frac{(\gamma^*)^{-1} |\gamma|^{2n+\delta}}{(n-1)!(n-1+\delta)!} e^{-\frac{\Gamma^2}{2}} L_{n+\delta-1}^{(0)}(\Gamma^2) \\ - \frac{\Gamma^2}{2} \mathcal{N}_n \mathcal{N}_{n-1} \sum_{n=0}^{\infty} \frac{(\gamma^*)^{-1} |\gamma|^{2n+\delta}}{(n-1)!(n+\delta)!} e^{-\frac{\Gamma^2}{2}} L_{n+\delta-1}^{(1)}(\Gamma^2).$$

$$\langle a^2 b^2 \rangle = \frac{|\lambda|^2}{2} [(1 + |\langle \sigma_x \rangle_w|^2) P_{41} + (1 - |\langle \sigma_x \rangle_w|^2) P_{42}], \quad (\text{A4})$$

$$P_{41} = \gamma^2,$$

$$P_{42} = \mathcal{N}_n \mathcal{N}_{n-2} \sum_{n=0}^{\infty} \frac{(\gamma^*)^{-2} |\gamma|^{2n+\delta}}{(n-2)!(n-2+\delta)!} e^{-\frac{\Gamma^2}{2}} L_{n+\delta-2}^{(0)}(\Gamma^2) \\ - \Gamma^2 \mathcal{N}_n \mathcal{N}_{n-2} \sum_{n=0}^{\infty} \frac{(\gamma^*)^{-2} |\gamma|^{2n+\delta}}{(n-2)!(n-1+\delta)!} e^{-\frac{\Gamma^2}{2}} L_{n+\delta-2}^{(1)}(\Gamma^2) \\ + \frac{\Gamma^4}{4} \mathcal{N}_n \mathcal{N}_{n-2} \sum_{n=0}^{\infty} \frac{(\gamma^*)^{-2} |\gamma|^{2n+\delta}}{(n-2)!(n+\delta)!} e^{-\frac{\Gamma^2}{2}} L_{n+\delta-2}^{(2)}(\Gamma^2).$$

$$\langle a^\dagger a b^\dagger b \rangle = \frac{|\lambda|^2}{2} [(1 + |\langle \sigma_x \rangle_w|^2) P_{51} + (1 - |\langle \sigma_x \rangle_w|^2) P_{52}], \quad (\text{A5})$$

$$P_{51} = |\gamma|^2 + \frac{\Gamma^2}{4} \frac{|\gamma| I_{\delta+1}(2|\gamma|)}{I_\delta(2|\gamma|)},$$

$$P_{52} = \mathcal{N}_n^2 \sum_{n=0}^{\infty} \frac{|\gamma|^{2n+\delta}}{(n-1)!(n+\delta-1)!} e^{-\frac{\Gamma^2}{2}} L_{n+\delta}^{(0)}(\Gamma^2) \\ - \frac{\Gamma^2}{2} \mathcal{N}_n^2 \sum_{n=0}^{\infty} \frac{|\gamma|^{2n+\delta}}{(n-1)!(n+\delta)!} e^{-\frac{\Gamma^2}{2}} L_{n+\delta}^{(1)}(\Gamma^2) \\ + \frac{\Gamma^2}{2} \mathcal{N}_n^2 \sum_{n=0}^{\infty} \frac{|\gamma|^{2n+\delta}}{(n-1)!(n+\delta)!} e^{-\frac{\Gamma^2}{2}} L_{n+\delta-1}^{(1)}(\Gamma^2) \\ + \frac{\Gamma^2}{4} \mathcal{N}_n^2 \sum_{n=0}^{\infty} \frac{|\gamma|^{2n+\delta}}{(n-1)!(n+\delta)!} e^{-\frac{\Gamma^2}{2}} L_{n+\delta}^{(0)}(\Gamma^2).$$

$$\langle a^\dagger b \rangle = \frac{|\lambda|^2}{2} (1 - |\langle \sigma_x \rangle_w|^2) I_{11}, \quad (\text{A6})$$

$$I_{11} = \Gamma^2 \mathcal{N}_n \mathcal{N}_{n-1} \sum_{n=0}^{\infty} \frac{(\gamma^*)^{-1} |\gamma|^{2n+\delta}}{(n-1)!(n+\delta)!} e^{-\frac{\Gamma^2}{2}} L_{(n+\delta-1)}^{(2)}(\Gamma^2) \\ - \frac{\Gamma^2}{2} \mathcal{N}_n \mathcal{N}_{n-1} \sum_{n=0}^{\infty} \frac{(\gamma^*)^{-1} |\gamma|^{2n+\delta}}{(n-1)!(n+\delta)!} e^{-\frac{\Gamma^2}{2}} L_{(n+\delta-1)}^{(1)}(\Gamma^2).$$

$$\langle a^2 \rangle = \frac{|\lambda|^2}{2} \left[(1 + |\langle \sigma_x \rangle_w|^2) \frac{\Gamma^2}{4} + (1 - |\langle \sigma_x \rangle_w|^2) I_{21} \right], \quad (\text{A7})$$

$$\begin{aligned} I_{21} &= \Gamma^2 \mathcal{N}_n^2 \sum_{n=0}^{\infty} \frac{|\gamma|^{2n+\delta}}{n!(n+\delta)!} e^{-\frac{\Gamma^2}{2}} L_{(n+\delta-2)}^{(2)}(\Gamma^2) \\ &+ \Gamma^2 \mathcal{N}_n^2 \sum_{n=0}^{\infty} \frac{|\gamma|^{2n+\delta}}{n!(n+\delta)!} e^{-\frac{\Gamma^2}{2}} L_{(n+\delta-1)}^{(1)}(\Gamma^2) \\ &+ \frac{\Gamma^2}{4} \mathcal{N}_n^2 \sum_{n=0}^{\infty} \frac{|\gamma|^{2n+\delta}}{n!(n+\delta)!} e^{-\frac{\Gamma^2}{2}} L_{(n+\delta)}^{(0)}(\Gamma^2). \end{aligned}$$

$$\langle b^2 \rangle = \frac{|\lambda|^2}{2} [(1 - |\langle \sigma_x \rangle_w|^2) I_{31}], \quad (\text{A8})$$

$$I_{31} = \mathcal{N}_n \mathcal{N}_{n-2} \sum_{n=0}^{\infty} \frac{(\gamma^*)^{-2} |\gamma|^{2n+\delta}}{(n-2)!(n+\delta)!} \Gamma^2 L_{n+\delta-2}^{(2)}(\Gamma^2) e^{-\frac{\Gamma^2}{2}}.$$

$$\langle a \rangle = \frac{|\lambda|^2}{2} [\Gamma \text{Re}[\langle \sigma_x \rangle_w] - 2i \Im[\langle \sigma_x \rangle_w] I_{41}], \quad (\text{A9})$$

$$\begin{aligned} I_{41} &= -\Gamma \mathcal{N}_n^2 \sum_{n=0}^{\infty} \frac{|\gamma|^{2n+\delta}}{n!(n+\delta)!} e^{-\frac{\Gamma^2}{2}} L_{(n+\delta-1)}^{(1)}(\Gamma^2) \\ &- \frac{\Gamma}{2} \mathcal{N}_n^2 \sum_{n=0}^{\infty} \frac{|\gamma|^{2n+\delta}}{n!(n+\delta)!} e^{-\frac{\Gamma^2}{2}} L_{(n+\delta)}^{(0)}(\Gamma^2). \end{aligned}$$

$$\langle b \rangle = -i |\lambda|^2 \text{Im}[\langle \sigma_x \rangle_w] I_{51}, \quad (\text{A10})$$

$$I_{51} = \Gamma \mathcal{N}_n \mathcal{N}_{n-1} \sum_{n=0}^{\infty} \frac{(\gamma^*)^{-1} |\gamma|^{2n+\delta}}{(n-1)!(n+\delta)!} e^{-\frac{\Gamma^2}{2}} L_{(n+\delta-1)}^{(1)}(\Gamma^2).$$

$$\langle a^{\dagger 2} a^2 \rangle = \frac{|\lambda|^2}{2} [(1 + |\langle \sigma_x \rangle_w|^2) K_{11} + (1 - |\langle \sigma_x \rangle_w|^2) K_{12}], \quad (\text{A11})$$

$$K_{11} = \frac{|\gamma|^2 I_{\delta-2}(2|\gamma|)}{I_{\delta}(2|\gamma|)} + \Gamma^2 \frac{|\gamma| I_{\delta-1}(2|\gamma|)}{I_{\delta}(2|\gamma|)} + \frac{\Gamma^4}{16},$$

$$K_{12} = \mathcal{N}_n^2 \sum_{n=0}^{\infty} \frac{|\gamma|^{2n+\delta}}{n!(n+\delta-2)!} e^{-\frac{\Gamma^2}{2}} L_{n+\delta}^{(0)}(\Gamma^2)$$

$$- \Gamma \mathcal{N}_n^2 \sum_{n=0}^{\infty} \frac{|\gamma|^{2n+\delta}}{n!(n+\delta-1)!} e^{-\frac{\Gamma^2}{2}} \Gamma L_{(n+\delta)}^{(1)}(\Gamma^2) + \Gamma \mathcal{N}_n^2 \sum_{n=0}^{\infty} \frac{|\gamma|^{2n+\delta}}{n!(n+\delta)!} (n+\delta-1) e^{-\frac{\Gamma^2}{2}} \Gamma L_{(n+\delta-1)}^{(1)}(\Gamma^2)$$

$$+ \frac{\Gamma^2}{4} \mathcal{N}_n^2 \sum_{n=0}^{\infty} \frac{|\gamma|^{2n+\delta}}{n!(n+\delta)!} e^{-\frac{\Gamma^2}{2}} \Gamma^2 L_{(n+\delta)}^{(2)}(\Gamma^2) + \frac{\Gamma^2}{4} \mathcal{N}_n^2 \sum_{n=0}^{\infty} \frac{|\gamma|^{2n+\delta}}{n!(n+\delta)!} e^{-\frac{\Gamma^2}{2}} \Gamma^2 L_{(n+\delta-2)}^{(2)}(\Gamma^2)$$

$$+ \Gamma^2 \mathcal{N}_n^2 \sum_{n=0}^{\infty} \frac{|\gamma|^{2n+\delta}}{n!(n+\delta-1)!} e^{-\frac{\Gamma^2}{2}} L_{(n+\delta)}^{(0)}(\Gamma^2) - \frac{\Gamma^3}{4} \mathcal{N}_n^2 \sum_{n=0}^{\infty} \frac{|\gamma|^{2n+\delta}}{n!(n+\delta)!} e^{-\frac{\Gamma^2}{2}} \Gamma L_{(n+\delta)}^{(1)}(\Gamma^2)$$

$$+ \frac{\Gamma^3}{4} \mathcal{N}_n^2 \sum_{n=0}^{\infty} \frac{|\gamma|^{2n+\delta}}{n!(n+\delta)!} e^{-\frac{\Gamma^2}{2}} \Gamma L_{(n+\delta-1)}^{(1)}(\Gamma^2) + \frac{\Gamma^4}{16} \mathcal{N}_n^2 \sum_{n=0}^{\infty} \frac{|\gamma|^{2n+\delta}}{n!(n+\delta)!} e^{-\frac{\Gamma^2}{2}} L_{(n+\delta)}^{(0)}(\Gamma^2).$$

$$\begin{aligned} \langle b^{\dagger 2} b^2 \rangle &= \frac{|\lambda|^2}{2} [(1 + |\langle \sigma_x \rangle_w|^2) K_{21} + (1 - |\langle \sigma_x \rangle_w|^2) K_{22}], \\ K_{21} &= \frac{|\gamma|^2 I_{\delta+2}(2|\gamma|)}{I_{\delta}(2|\gamma|)}, \\ K_{22} &= \mathcal{N}_n^2 \sum_{n=0}^{\infty} \frac{|\gamma|^{2n+\delta}}{(n-2)!(n+\delta)!} e^{-\frac{\Gamma^2}{2}} L_{(n+\delta)}^{(0)}(\Gamma^2). \end{aligned} \quad (\text{A12})$$

-
- [1] A. I. Lvovsky, P. Grangier, A. Ourjoumtsev, V. Parigi, M. Sasaki, and R. Tualle-Broui, (2020), [arXiv:2006.16985 \[quant-ph\]](#).
- [2] M. Walschaers, [PRX Quantum](#) **2**, 030204 (2021).
- [3] W. Asavanant and A. Furusawa, [Phys. Rev. A](#) **109**, 040101 (2024).
- [4] C. Wang, Y. Y. Gao, P. Reinhold, R. W. Heeres, N. Ofek, K. Chou, C. Axline, M. Reagor, J. Blumoff, K. M. Sliwa, L. Frunzio, S. M. Girvin, L. Jiang, M. Mirrahimi, M. H. Devoret, and R. J. Schoelkopf, [Science](#) **352**, 1087 (2016).
- [5] I. Afek, O. Ambar, and Y. Silberberg, [Science](#) **328**, 879 (2010).
- [6] H. Wang, M. Mariantoni, R. C. Bialczak, M. Lenander, E. Lucero, M. Neeley, A. D. O’Connell, D. Sank, M. Weides, J. Wenner, T. Yamamoto, Y. Yin, J. Zhao, J. M. Martinis, and A. N. Cleland, [Phys. Rev. Lett.](#) **106**, 060401 (2011).
- [7] L. Dao-ming, [Int. J. Theor. Phys.](#) **54**, 2289 (2015).
- [8] M. Riabinin, P. R. Sharapova, T. J. Bartley, and T. Meier, [J. Phys. Commun.](#) **5**, 045002 (2021).
- [9] G. S. Agarwal, [Phys. Rev. Lett.](#) **57**, 827 (1986).
- [10] K. Tara and G. S. Agarwal, [Phys. Rev. A](#) **50**, 2870 (1994).
- [11] A. Gábris and G. S. Agarwal, [Int. J. Quantum Inf.](#) **05**, 17 (2007).
- [12] C. Zhou, W. Bao, and X. Fu, [Sci. China Inf. Sci.](#) **53**, 2485 (2010).
- [13] K. P. Seshadreesan, J. P. Dowling, and G. S. Agarwal, [Phys. Scr.](#) **90**, 074029 (2015).
- [14] H. Vahlbruch, M. Mehmet, K. Danzmann, and R. Schnabel, [Phys. Rev. Lett.](#) **117**, 110801 (2016).
- [15] L. Wang and S. Zhao, [Quantum Inf. Process.](#) **16**, 100 (2017).
- [16] F. Acernese, Agathos, and et al. (Virgo Collaboration), [Phys. Rev. Lett.](#) **123**, 231108 (2019).
- [17] T. Q. Dat, [Int. J. Theor. Phys.](#) **62**, 41 (2023).
- [18] V. Roman-Rodriguez, D. Fainsin, G. L. Zanin, N. Treps, E. Diamanti, and V. Parigi, [Phys. Rev. Res.](#) **6**, 043113 (2024).
- [19] L. Hong, [Phys. Lett. A](#) **264**, 265 (1999).
- [20] L. Hong and G. Guang-can, [Acta Phys. Sinica \(Overseas Edition\)](#) **8**, 577 (1999).
- [21] A. Kitagawa, M. Takeoka, M. Sasaki, and A. Chefles, [Phys. Rev. A](#) **73**, 042310 (2006).
- [22] A. Biswas and G. S. Agarwal, [Phys. Rev. A](#) **75**, 032104 (2007).
- [23] H.-C. Yuan, X.-X. Xu, and H.-Y. Fan, [Int. J. Theor. Phys.](#) **48**, 3596 (2009).
- [24] D. M. Truong, H. T. X. Nguyen, and A. B. Nguyen, [Int. J. Theor. Phys.](#) **53**, 899 (2014).
- [25] N. T. X. Hoai and T. M. Duc, [Int. J. Mod. Phys. B](#) **30**, 1650032 (2016).
- [26] H.-C. Yuan, X.-X. Xu, and Y.-J. Xu, [Optik](#) **172**, 1034 (2018).
- [27] D.-M. Lu, [Int. J. Theor. Phys.](#) **57**, 2767 (2018).
- [28] T. M. Duc, D. H. Dinh, and T. Q. Dat, [J. Phys. B](#) **53**, 025402 (2019).
- [29] T. M. Duc, T. Q. Dat, and H. S. Chuong, [Int. J. Mod. Phys. B](#) **34**, 2050223 (2020).
- [30] D. M. Truong, C. S. Ho, and D. Q. Tran, [J. Comput. Electron.](#) **20**, 2124 (2021).
- [31] H. S. Chuong and T. M. Duc, [J. Phys. B](#) **56**, 205401 (2023).
- [32] V. Parigi, A. Zavatta, M. Kim, and M. Bellini, [Science](#) **317**, 1890 (2007).
- [33] K. Sanaka, K. J. Resch, and A. Zeilinger, [Phys. Rev. Lett.](#) **96**, 083601 (2006).
- [34] H. M. Wiseman and G. J. Milburn, *Quantum Measurement and Control* (Cambridge University Press, Cambridge, England, 2014).
- [35] Y. Aharonov, D. Z. Albert, and L. Vaidman, [Phys. Rev. Lett.](#) **60**, 1351 (1988).
- [36] B. Tamir and E. Cohen, [Quanta](#) **2**, 7 (2013).
- [37] B. Svensson, [Quanta](#) **2**, 18 (2013).
- [38] J. Harris, R. W. Boyd, and J. S. Lundeen, [Phys. Rev. Lett.](#) **118**, 070802 (2017).
- [39] A. G. Kofman, S. Ashhab, and F. Nori, [Phys. Rep.](#) **520**, 43 (2012), nonperturbative theory of weak pre- and post-selected measurements.
- [40] J. Dressel, M. Malik, F. M. Miatto, A. N. Jordan, and R. W. Boyd, [Rev. Mod. Phys.](#) **86**, 307 (2014).
- [41] Q. Hu, T. Yusufu, and Y. Turek, [Phys. Rev. A](#) **105**, 022608 (2022).
- [42] W. J. Xu, T. Yusufu, and Y. Turek, [Phys. Rev. A](#) **105**, 022210 (2022).
- [43] Y. Turek, A. Islam, and A. Abliz, [Eur. Phys. J. Plus](#) **138**, 72 (2023).
- [44] G. S. Agarwal, [J. Opt. Soc. Am. B](#) **5**, 1940 (1988).
- [45] J. M. Gertler, S. van Geldern, S. Shirol, L. Jiang, and C. Wang, [PRX Quantum](#) **4**, 020319 (2023).
- [46] S.-C. Gou, J. Steinbach, and P. L. Knight, [Phys. Rev. A](#) **54**, 4315 (1996).
- [47] S.-B. Zheng, [Czechoslov. J. Phys.](#) **52**, 713 (2002).
- [48] A.-S. Obada and E. Khalil, [Opt. Commun.](#) **260**, 19 (2006).
- [49] Y.-L. Dong, X.-B. Zou, and G.-C. Guo, [Phys. Lett. A](#) **372**, 5677 (2008).

- [50] C. C. Gerry, J. Mimih, and R. Birrittella, *Phys. Rev. A* **84**, 023810 (2011).
- [51] H. Jeon, J. Kang, J. Kim, W. Choi, K. Kim, and T. Kim, *Sci. Rep.* **14**, 6847 (2024).
- [52] C. T. Lee, *Phys. Rev. A* **41**, 1569 (1990).
- [53] A.-S. F. Obada, M. M. A. Ahmed, and S. Sanad, *J. Phys. Commun.* **4**, 015008 (2020).
- [54] A. GÁBRIS and G. S. AGARWAL, *Int. J. Quantum Inf.* **05**, 17 (2007).
- [55] V. V. Albert, S. O. Mundhada, A. Grimm, S. Touzard, M. H. Devoret, and L. Jiang, *Quantum Sci. Technol.* **4**, 035007 (2019).
- [56] U. Andersen, G. Leuchs, and C. Silberhorn, *Laser Photonics Rev.* **4**, 337 (2010).
- [57] R. Schnabel, *Phys. Rep.* **684**, 1 (2017), squeezed states of light and their applications in laser interferometers.
- [58] G. Agarwal, *Quantum Optics* (Cambridge University Press, Cambridge, England, 2013).
- [59] M. Hillery, *Phys. Rev. A* **40**, 3147 (1989).
- [60] W. K. Lai, V. Buek, and P. L. Knight, *Phys. Rev. A* **44**, 6043 (1991).
- [61] A. M. Bhargav, A. Wahid, S. Das, and V. G. Achanta, *MAPAN* **38**, 997 (2023).
- [62] H. Paul, *Rev. Mod. Phys.* **54**, 1061 (1982).
- [63] B. Lounis and M. Orrit, *Rep. Prog. Phys.* **68**, 1129 (2005).
- [64] G. S. Agarwal and A. Biswas, *J. Opt. B: Quantum Semi-class. Opt.* **7**, 350 (2005).
- [65] M. Hillery and M. S. Zubairy, *Phys. Rev. Lett.* **96**, 050503 (2006).
- [66] F. Li, T. Li, and G. S. Agarwal, *Phys. Rev. Res.* **3**, 033095 (2021).
- [67] L.-M. Duan, G. Giedke, J. I. Cirac, and P. Zoller, *Phys. Rev. Lett.* **84**, 2722 (2000).
- [68] G. Ren, W. hai Zhang, and Y. jun Xu, *Physica A* **520**, 106 (2019).
- [69] If the eigenvalue function of system observable \hat{A} is $\hat{A}|a_i\rangle = a_i|a_i\rangle$, then conditionally expectation value of \hat{A} for preselected state $|\psi_i\rangle$ and postselected state $|\psi_f\rangle$ can be written as
- $$\langle \hat{A} \rangle_c = \frac{\sum_i a_i |\langle \psi_f | a_i \rangle \langle a_i | \psi_i \rangle|^2}{\sum_j |\langle \psi_f | a_j \rangle \langle a_j | \psi_i \rangle|^2}$$
- [70] P. Kok, W. J. Munro, K. Nemoto, T. C. Ralph, J. P. Dowling, and G. J. Milburn, *Rev. Mod. Phys.* **79**, 135 (2007).
- [71] X.-Y. Xu, Y. Kedem, K. Sun, L. Vaidman, C.-F. Li, and G.-C. Guo, *Phys. Rev. Lett.* **111**, 033604 (2013).
- [72] J. Zhu, Z. Li, Y. Liu, Y. Ye, Q. Ti, Z. Zhang, and F. Gao, *Phys. Rev. A* **103**, 032212 (2021).
- [73] C.-W. Wu, J. Zhang, Y. Xie, B.-Q. Ou, T. Chen, W. Wu, and P.-X. Chen, *Phys. Rev. A* **100**, 062111 (2019).
- [74] Y. Pan, J. Zhang, E. Cohen, C.-w. Wu, P.-X. Chen, and N. Davidson, *Nat. Phys.* **16**, 1206 (2020).
- [75] W. Su, M. Zhang, C. Wu, Y. Xie, H. Hu, T. Chen, T. Zhan, B. Ou, W. Wu, J. Zhang, and P. Chen, *Phys. Rev. A* **108**, 042601 (2023).
- [76] C. Wu, H. Hu, J. Zhang, W. Su, M. Zhang, T. Zhan, Q. Qin, W. Wu, and P. Chen, *Phys. Rev. A* **109**, 032211 (2024).
- [77] Y.-S. Ra, A. Dufour, M. Walschaers, C. Jacquard, T. Michel, C. Fabre, and N. Treps, *Nat. Phys.* **16**, 144 (2020).